UNCLASSIFIED

SECURITY CLASSIFICATION OF THIS PAGE (When Data Entered)

DTIC FILE COPY

(1)

AD-A197 223

REPORT DOCUMENTATION PAGE

READ INSTRUCTIONS BEFORE COMPLETING FORM

1. REPORT NUMBER: AFIT/CI/NR 88-181

2. GOVT ACCESSION NO.

3. RECIPIENT'S CATALOG NUMBER

TITLE (and Subtitle): A GLOBAL ANALYSIS AND CORRELATION OF NIMBUS 7 CLOUD AND LONGWAVE RADIATION DATA

5. TYPE OF REPORT & PERIOD COVERED: MS THESIS

6. PERFORMING ORG. REPORT NUMBER

AUTHOR(s): DEANNA RITA RAMIREZ

8. CONTRACT OR GRANT NUMBER(s)

PERFORMING ORGANIZATION NAME AND ADDRESS: AFIT STUDENT AT: COLORADO STATE UNIVERSITY

10. PROGRAM ELEMENT, PROJECT, TASK AREA & WORK UNIT NUMBERS

CONTROLLING OFFICE NAME AND ADDRESS

12. REPORT DATE: 1988

13. NUMBER OF PAGES: 75

14. MONITORING AGENCY NAME & ADDRESS (if different from Controlling Office): AFIT/NR, Wright-Patterson AFB OH 45433-6583

15. SECURITY CLASS. (of this report): UNCLASSIFIED

15a. DECLASSIFICATION/DOWNGRADING SCHEDULE

16. DISTRIBUTION STATEMENT (of this Report)

DISTRIBUTED UNLIMITED: APPROVED FOR PUBLIC RELEASE

17. DISTRIBUTION STATEMENT (of the abstract entered in Block 20, if different from Report)

SAME AS REPORT

18. SUPPLEMENTARY NOTES

Approved for Public Release: IAW AFR 190-1
LYNN E. WOLAVER Lynn Wolaver 8 Aug 88
Dean for Research and Professional Development
Air Force Institute of Technology
Wright-Patterson AFB OH 45433-6583

19. KEY WORDS (Continue on reverse side if necessary and identify by block number)

20. ABSTRACT (Continue on reverse side if necessary and identify by block number)

ATTACHED

DTIC ELECTE AUG 1 7 1988 S D H

DD FORM 1 JAN 73 1473 EDITION OF 1 NOV 65 IS OBSOLETE

UNCLASSIFIED

SECURITY CLASSIFICATION OF THIS PAGE (When Data Entered)

88 8 16 030

THESIS

A GLOBAL ANALYSIS AND CORRELATION OF NIMBUS 7 CLOUD AND LONGWAVE RADIATION DATA

Submitted by
Deanna Rita Ramirez
Department of Atmospheric Science

In partial fulfillment of the requirements
for the Degree of Master of Science
Colorado State University
Fort Collins, Colorado
Summer, 1988

COLORADO STATE UNIVERSITY

May 24, 1988

WE HEREBY RECOMMEND THAT THE THESIS PREPARED UNDER OUR SUPERVISION BY DEANNA RITA RAMIREZ ENTITLED "A GLOBAL ANALYSIS AND CORRELATION OF NIMBUS 7 CLOUD AND LONGWAVE RADIATION DATA" BE ACCEPTED AS FULFILLING IN PART REQUIREMENTS FOR THE DEGREE OF MASTER OF SCIENCE.

Committee on Graduate Work

Howard Finger

William M. Gray

Thomas H. Vonder Haar

Adviser

William S. Cotton (Acting)

Department Head

ABSTRACT

A GLOBAL ANALYSIS AND CORRELATION OF NIMBUS 7 CLOUD AND LONGWAVE RADIATION DATA

Cloud data obtained from the Temperature Humidity Infrared Radiometer and Total Ozone Mapping Spectrometer and longwave radiation obtained from the Earth Radiation Budget instrument, all aboard the NIMBUS 7 satellite, have been used to present global analyses of the total cloud, high cloud and radiation fields and a correlation between the fields. The horizontal projections of the seasonal mean field for total and high cloud clearly depict the location and seasonal variation of the ITCZ by a maximum of cloud cover. The SH middle latitudes depict a zonal pattern of cloud amount for winter and summer, while the NH reveals an increase of cloud from summer to winter over the storm tracks. The dry subtropics are defined by a minimum of cloud cover. Areas of small or large amount of total cloud are defined by a small standard deviation, while the transition zones between maximum and minimum centers of total cloud are characterized by a large standard deviation. The standard deviation of the high cloud reveals that in areas of large high cloud amount, the variation of cloud is large due to the advective or convective processes with which the cloud is associated. For small amount of high cloud, the variation of the cloud is small.

Analyses of the global distribution of the seasonal mean field for infrared radiation (IR) indicate that areas that are defined by large high cloud amount are also characterized by low IR due to the low radiative temperatures of the high cloud. Large IR values correspond to the subtropical anticyclone and desert regions where the IR is related to the large radiative temperatures of the earth's surface. The middle latitudes are defined by a zonal pattern of IR in winter corresponding to the large north-south surface temperature gradient. The standard deviation field of IR indicates that in the cloudy regions of the low latitudes,

there is a large variation of IR responding to the large variation in high cloudiness. The dry subtropical regions are defined by a small IR variation. In the middle latitudes the standard deviation of IR is not well defined, but there is a slight increase of values over the storm tracks.

Regression analyses between the mean fields of IR and high cloud indicate the expected negative linear correlation in a region of the graph. However, a secondary "branch" emerges in the diagram relating low IR values to low high cloud amounts. These points represent the middle latitudes where low IR values are a result of the low surface temperatures at these latitudes, not only of the high cloud amount. The regression analyses between the standard deviation fields of IR and high cloud indicate the expected positive correlation but with a bulge of data points disrupting the linear trend. These points represent the middle latitudes where the variation of IR is a result of the variation of emitted radiation from the surface as well as the high cloud.

The difference between determined maximum IR values, corresponding to days of minimum total cloud cover found over a region, and measured IR values results in the IR emitted by the cloud itself (Δ IR). Regression analyses between IR and total cloud for low latitude regions of cloud transition zones present a nearly poistive linear trend. These areas are characterized by a large variation in cloud, and the cloud IR responds to this variation. The regression analyses in dry regions of the low latitudes depict a cluster of data points corresponding to low cloud amount and low values of IR emitted by the cloud. This indicates that the determined maximum IR is very near the maximum possible IR and that there is a small variation of cloud and IR. Cloudy regions of the low latitudes depict, in part, a positive correlation between total cloud and ΔIR but also indicate small amount of IR emitted by cloud correlated with large cloud amounts. This is a result of a decrease in high cloud amount (small ΔIR) but with a large amount of lower altitude cloud still present.

Deanna Rita Ramirez
Department of Atmospheric Science
Colorado State University
Fort Collins, Colorado 80523
Summer, 1988

ACKNOWLEDGEMENTS

The author wishes to thank Dr. Thomas H. Vonder Haar for his support and advice throughout the development of this research. This appreciation is also extended to Laura Smith and David Randel for their guidance and helpful discussions and to Andrew Jones for his exceptional programming support. Thanks also to Loretta Wilson for her patience in processing this thesis, to Judy Sorbie for her drafting support, and to Fredell Boston for her library assistance.

This research was supported by the United States Air Force/Air Force Institute of Technology.

Accession For
NTIS GRA&I ☑
DTIC TAB ☐
Unannounced ☐
Justification
By
Distribution/
Availability Codes
Avail and/or
Dist Special
A-1

TABLE OF CONTENTS

LIST OF FIGURES

1.0 INTRODUCTION

Knowledge of the global cloud cover is of key importance in understanding the Earth Radiation Budget and climate change. The largest day to day variations of albedo and outgoing longwave radiation from the earth-atmosphere system are strongly dependent on the variation in cloud cover. Numerous studies, both qualitative and quantitative, have been performed to examine the relationship between cloud parameters and the radiation budget. The results of some of these studies have been questioned due to uncertainties in observational data used in determining cloud parameters and deriving or validating the relationship between clouds and radiation.

When the NIMBUS 7 satellite was launched in October 1978, for the first time cloud parameters and radiation parameters could be determined simultaneously by separate instruments on the same satellite. Radiation data was obtained by the Earth Radiation Budget (ERB) Experiment instrument, and, initially only the Temperature Humidity Infrared Radiometer (THIR) was used to determine cloud fields. However, after evaluation of the cloud parameters, data from the Total Ozone Mapping Spectrometer (TOMS) instrument was used to improve the cloud estimates.

The aim of many investigations between cloud and radiation parameters is to present the effect of cloud amount on changes in the net radiation. However, my study is limited to the correlation of longwave flux with total and high altitude cloud. The purpose of my study is two-fold. First, I examine the cloud estimation algorithms and analyze the resulting global cloud product. Second, I examine the response of longwave radiation due to variation in cloud.

An initial attempt of studying the effects of middle and low altitude cloud on radiation parameters was disgarded because of inadequate satellite determinations of the lower altitude cloud cover.

2.0 CLOUD DATA SET

2.1 Data Sources

Data used in the cloud algorithms is acquired from two sources The satellite data used is obtained from instruments aboard the NIMBUS 7 satellite. The NIMBUS 7 was launched in October 1978 and set into a sun synchronous, polar orbit with an altitude of 955 km. The ascending node (AN) data originates from satellite equatorial crossings at local noon, and descending node (DN) data is from equatorial crossings at local midnight. Data for this paper includes only that from the AN. Auxilary data used was obtained from an automated cloud analysis model developed by the Air Force.

2.1.1 Satellite Data

Infrared (IR) radiances were obtained from the NIMBUS 7 Temperature Humidity Infrared Radiometer (THIR) instrument which is a two-channel scanning radiometer designed to measure earth radiation both day and night from two bands. A 10.5 μm to 12.5 μm (11.5 μm) window provides an image of the cloud cover and temperatures of the cloud tops, land, and ocean surfaces. A 6.5 μm to 7.0 μm (6.7 μm) channel provides information on the moisture and cirrus cloud content of the upper troposphere and stratosphere. The ground resolution at the subpoint is 6.7 km for the 11.5 μm channel and 20 km for the 6.7 μm channel.

The source of the reflectivity data used is the Total Ozone Mapping Spectrometer (TOMS) subsystem which is part of the Solar Backscatter Ultraviolet and Total Ozone Mapping Spectrometer (SBUV/TOMS) Experiment. The TOMS sub-system is a single monochrometer which has a 3 degree by 3 degree instantaneous field of view (IFOV) and measures the ultraviolet (UV) backscattered radiation in six discrete wavelengths ranging from 312.5 nm to 380 nm. The scanning design provides complete daily coverage of the

globe with the IFOV varying from 50 km by 50 km at the nadir to 150 km by 200 km in the extreme off nadir position.

2.1.2 Auxilary Data

Auxilary data was taken from the Air Force Three-Dimensional Nephanalysis (AF 3-D Neph) which is an automated cloud analysis model which uses a combination of satellite, surface, and upper air observations and pilot reports to produce a high resolution three-dimensional cloud analysis over the globe. The data include terrain height analysis, snow/ice analysis, and temperature analysis over the globe.

The terrain height analysis is reported in tenths of meters. The snow/ice data is acquired from conventional surface reports, weekly Navy sea ice analysis, satellite radiometer observations, and climatology. The surface temperature analysis over land was prepared using conventional shelter reports from every three hours. Sea surface temperture measurements taken from ship reports every six hours and from satellite remote sensing twice a day are used for the surfae temperature analysis over water.

2.2 Cloud Detection Algorithms

An initial attempt at deriving clouds from only THIR and climatological information presented questionable results. To improve cloud estimations, three algorithms were developed using, in addition to the THIR radiance data, reflectivity data from the TOMS instrument and AF 3-D Neph data. The parameters used in these algorithms are determined for each of 18,630 sub-target areas (STA) over the globe measuring about 165 km by 165 km each.

2.2.1 Infrared (IR) Algorithm

The IR algorithm is used to classify the each THIR 11.5 μm radiance observation (pixel) as being either clear, low, middle, or high altitude cloud depending on its magnitude in comparison to precomputed threshold values. The cloud/no cloud threshold value is computed by determining the time interpolation of the AF surface temperature reported every three

hours and adjusting the temperature for atmospheric water vapor attenuation. This resulting temperature is the equivalent blackbody radiative temperature which should be detected by the 11.5 μm THIR observation. Then a range of temperatures within 95% probability (two standard deviation) of being clear is computed defining the cloud/no cloud threshold.

Cloud amount is determined by separating cloud covered fields of view (FOVs) from cloud-free fields based on their observed radiances. Each pixel is classified as clear or cloudy by the equation

$$T < TS - \Delta T$$

where T is the satellite measured radiance, TS is the clear sky radiance, ΔT is the threshold amount (two standard deviation). If the equation is true, the pixel is defined as cloudy. The fraction of cloud cover is determined by counting the number of cloudy pixels with the assumption that all cloudy pixels are 100% cloudy.

For the threshold separating low from middle cloud, an altitude of 2 km above mean sea level is used as defined in the International Cloud Atlas. The temperature at 2 km, T_L, is computed for each STA with the equation

$$T_L = T_{AF} + (2 - Z_0)(dT/dZ_L)$$

where dT/dZ_L is the climatological lapse rate between the surface and 2 km, Z_0 is the altitude of the suface above mean sea level, and T_{AF} is the surface temperature.

For the threshold separating middle and high cloud, the altitude varies poleward of 30 degrees latitude according to

$$Z = 7 - 1.5\ (1 - \cos\left[3\,(\mathrm{LAT} - 30)\right])\,.$$

Equatorward of 30 degrees latitude, $Z_M = 7$ km as defined by the International Cloud Atlas. The temperature threshold separating middle from high cloud is given by the equation

$$T_M = T_L + (Z_M - 2)(dT/dZ_M)$$

where dT/dZ_M is the climatological lapse rate between 2 km and the reference altitude Z_r. The value of Z_r is 7 km between 0 and 30 degrees latitude, 6 km betweeen 30 and 60 degrees, and 4 km for latitudes greater than 60 degrees.

Random and systematic errors occur during the adjustment of temperature for attenuation and in the calculation of the threshold values. These errors are due to lack of data over tropical oceans, horizontal variations of surface temperature within a STA, and partially filled FOVs of the radiometer. Errors due to partially filled FOVs result from observations of clouds smaller than a FOV or clouds which are aligned so that they fall along edges of a FOV. This leads to an overestimation of cloud cover since any FOV partially covered is assumed to be completely cloudy.

2.2.2 Ultraviolet (UV) Algorithm

An additional and independent estimate of cloud cover is determined by using reflectivity data from TOMS. The average reflectivity of all FOVs within a STA is used to determine the total cloud cover within that STA as long as the surface is not covered by snow or ice. This algorithm was developed for the purpose of better detecting low cloud which has a radiative temperature similar to the surface below. In many cases, the IR algorithm cannot distinguish low cloud from the surface which results in an underestimation of cloud cover for these areas.

Cloud amount for a STA is determined by the UV algorithm from a linear relationship of the average STA UV reflectivity and IR cloud amount if the STA is not ice covered or snow covered. Figure 2.1 shows this relationship. The correlation is not exactly linear, but it shows a trend of TOMS reflectivity increasing between 8% and 50% as cloud amount increases from 0% to 100%. The line of best fit for the linear regression indicates that for low cloud amounts, the line lies below the data points. This is because the IR algorithm underestimates the amount of cloud for low cloud amounts. The regression line also lies below the data for 100% cloud cover. This is because, as cloud amount increases, there is a larger concentration of high altitude clouds in comparison to low altitude clouds. These high clouds are more reflective due to their geometrical thickness. Since the UV algorithm is used when the IR algorithm detects low cloud or no cloud (section 2.2.3), a maximum

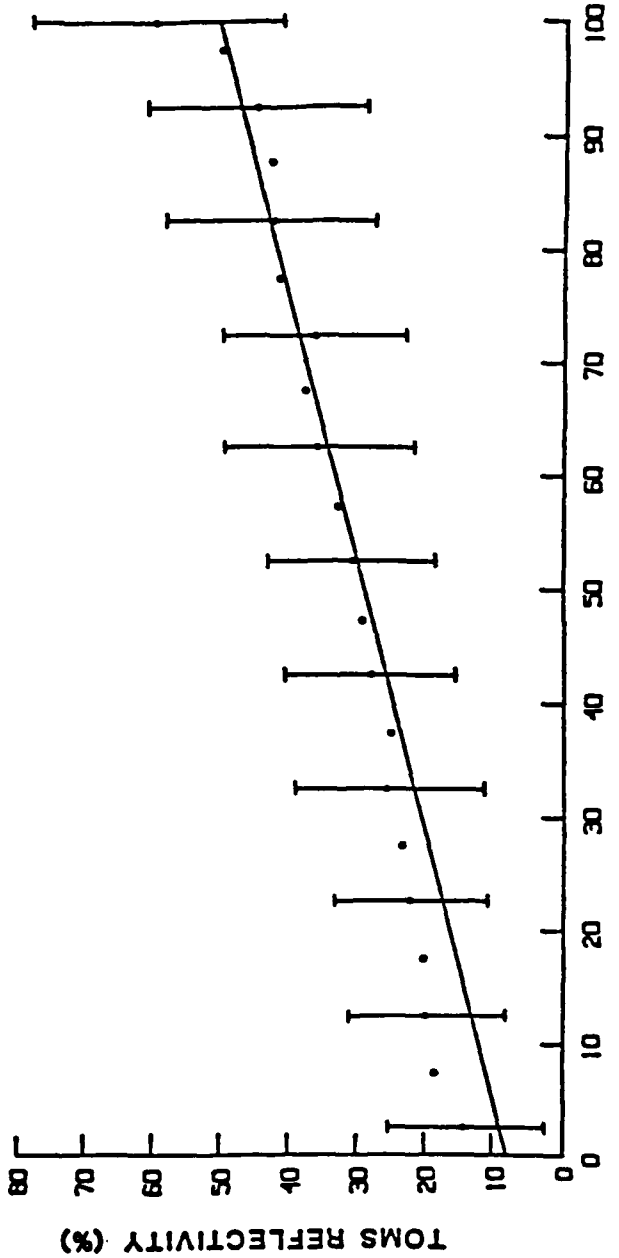

Figure 2.1 TOMS reflectivity as a function of IR cloud amount.

reflectivity of 50% (instead of the 80% shown by the data points) was chosen. This value is more representative of reflectivity for low altitude clouds.

2.2.3 Bispectral Algorithm

The bispectral algorithm was developed to combine the best estimates of cloud cover as independently determined by IR and UV algorithms. The result is the most accurate determination of total cloud cover. The IR algorithm presents the better estimate of middle and high cloud cover since the thermal contrast between the surface and the cloud is large. The UV estimate of cloud is more accurate for low cloud or no cloud due to the small thermal contrast betweeen the cloud and surface.

The bispectral algorithm approaches the IR total cloud estimate when a large amount of middle and high cloud is present and approaches the UV total cloud estimate for a large amount of low cloud or no cloud. The bispectral algorithm is represented by the expression

$$NCLE = BCLE * (1 - W) + TOMS * W$$

where $NCLE$ represents the New Cloud data (bispectral algorithm product) and $BCLE$ represents the Basic Cloud data (IR algorithm product). The total weight, W, is a composite of the two weights, W_1 and W_2. W_1 reduces the weight of the cloud estimation as the satellite zenith angle (θ) increases, because with increased θ, the size of the TOMS FOV becomes larger than the STA (THIR FOV remains constant). This creates less reliability in the TOMS cloud estimation. Cosine (θ) represents the reduction in the number of TOMS FOVs within a STA. W_2 represents the fraction of the STA, as estimated by THIR, to be clear or covered with low cloud. The larger the estimate of low cloud or clear sky, the closer the cloud estimation as determined by the NCLE will be to the TOMS estimate. The smaller the estimate, the closer the NCLE estimation will be to the BCLE.

2.3 Validation

Both quantitative and qualitative validations have been performed on the NIMBUS 7 cloud algorithms. Quantitative validations included an analysis of the auxilary data

used for the cloud algorithms, computations of the sensitivity and expected errors in total cloud amount due to uncertainties of parameters for each of the three algorithms, and a statistical comparison with an analyst's estimates derived from independent, concurrent Geosynchronous (GOES) satellite images along with meteorological reports. Qualitative validation involved comparison of images of NIMBUS 7 cloud estimates with simultaneous visible and IR GOES satellite images.

It was found that AF surface temperature data was suitable for use in the cloud algorithms, except over Antarctica where temperatures were found to be 40 to 60 degrees celcius to high. As a result, climotologial temperatures were used over areas south of 63 degrees south. Also, since AF temperatures are taken in shelters, the actual surface (skin) temperatures over hot, dry land areas can be as much as 40 degrees celcius higher, however, the AF temperatures were found to be useful. The AF snow/ice fields were found to be adequate for identifying areas where the TOMS algorithm can not be used in cloud estimation.

Error and sensitivity analysis of the algorithms showed that for the TOMS algorithm, the uncertainty is least for small amounts of cloud ($\pm 7.9\%$) and greatest for large amounts of cloud ($\pm 36.6\%$). The error in the IR algorithm was found to be $\pm 10.8\%$ and is mainly a result of the amount of atmospheric attenuation. For the bispectral algorithm, the range of error in the clear sky case is 7.9% to 23.1% and in the overcast case is 10.8% to 17.7%.

Statistical comparison of AN data with an analyst revealed that for the IR algorithm, systematic errors in the mean were less than 14% and random errors ranged between 8% and 31%. The correlation coefficient exceeded .72 with a max of .95 over oceans. For the bispectral algorithm, the systematic errors were less than 8% and random errors ranged between 7% and 16%. The correlation coefficient exceeded .91 with a maximum of .96 over the oceans.

Qualitative comparison with satellite images revealed that the IR algorithm tends to underestimate cloud when the scene is covered by low level cloud and overestimate cloud when the area is covered with small scale cumulus, thin cirrus, or when over areas of excessive humidity. The latter two overestimations are due to attenuation of IR pixels. The bispectral algorithm showed good agreement in the location and amount of cloud cover. It was in especially good agreement for areas of thin cirrus and deep convective clouds.

2.4 Data Storage

The data derived from the IR, UV, and bispectral algorithms are processed into 2070 equal sized target areas measuring 500 km by 500 km. The data is archived weekly, and each year of data is stored on one magnetic tape. These tapes include more than 100 other parameters as well. The data set is referred to as the Cloud Matrix (CMATRIX) data, and was initiated in April 1979 when the AF surface temperatures became available and continued through March 1985.

2.5 Global Cloud Product

CMATRIX data for the global analyes of cloud is taken from the period June 1979 through May 1980. Discussion of the data over Antarctica is omitted because the cloud data is unreliable due to the difficulty of identifying clouds over ice and snow surfaces and the less adequate climatological data used for surface temperatures. In this section I will discuss the time series of total cloud over the globe. For a discussion of the cloud product for high, middle, and low altitude cloud, refer to appendices A through C.

Figure 2.2 shows the time-latitude cross section of the zonally averaged total cloud amount. The Intertropical Convergence Zone (ITCZ), a region of converging trade winds and heavy, convectvie precipitation, is depicted by the band of maximum total cloud cover along the equatorial region. It is shown to follow the interannual variation of solar radiation. Jun through Sep the ITCZ is found in the NH approximately between the equator and 12°N. During the transition period, Oct through Dec, the ITCZ is displaced southward until it is situated mostly in the SH by Jan. In Mar it begins its movement back to the NH.

The subtropics, dominated by the subtropical anticyclones, are areas of stable conditions where subsidence supresses convective activity. It is characterized by a minimum of total cloud cover. During the NH summer, the region of minimum cloudiness lies approximately between 20°N and 40°N. But as the NH winter season approaches, the boundry of this cloud-free area is pushed southward by middle latitude storm systems to occupy the latitude band 10°N to 30°N by Jan. In the SH, the minimum cloud region of the subtropics is located approximately between 10°S and 25°S during the SH winter. As the summmer approaches,

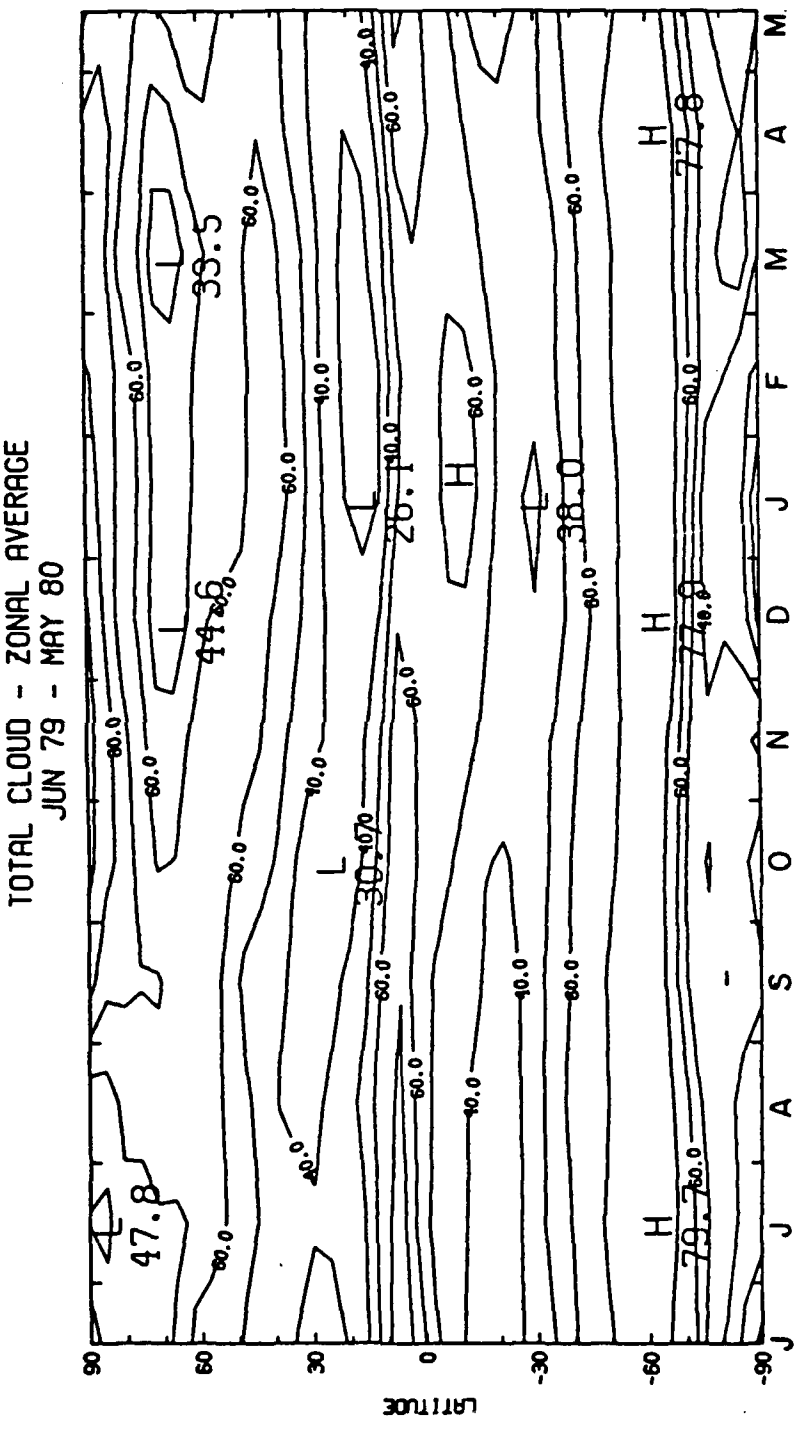

Figure 2.2 Time-latitude cross section of zonally averaged total cloud amount.

the equatorward edge of the subtropics deteriorates as the ITCZ moves from the NH into the SH. There is also an indication of the effects of the subtropics moving towards the South Pole with the slight retereat of middle latitude cloudiness.

The seasonal shift in total cloud cover is evident in the NH middle latitudes which are characterized by extratropical weather systems embedded within the westerlies of the polar vortex. During the winter seasons, this vortex expands and strengthens allowing migrating frontal systems and the associated cloud cover to extend southward. This is evident by the protruding tongue of total cloud cover > 60% between 40°N and 50°N between Oct and Apr. During the summer, the polar vortex weakens resulting in a decrease of total cloud within the middle latitudes. In the NH latitude belt approximately 50°N to 75°N, there appears a minimum of total cloud cover. This is due to the intense anticyclones which build over the massive continents during the winter within this latitude band.

The SH middle latitudes, in contrast to the NH, show little variation in time of the latitudinal position of total cloud cover. This is a result of the difference between hemispheres in the land to ocean ratio which is 50% in the NH and about 5% to 10% in the SH. The middle latitude winter cyclone systems are a result of the release of stored energy from the oceans. Assuming that the amount of energy released by the oceans of the hemispheres during the winter is about the same, the release of energy is more intense in the NH winter creating more intense cyclones than those in the SH. During the summer, the opposite situation occurs with abundant storage of energy in the NH oceans substantially weakening the cyclones. In the SH summer, the oceans store energy at slower rate allowing for only a small decrease in the cyclone intensity. The result is little seasonal variation of the total cloud cover in the SH middle latitudes.

The NH polar regions during the fall, winter, and spring months indicate total cloud cover to be greater than 70%, and as high as 90%. As the sun retreats to the SH for the NH winter, the surface temperature of this high latitude region becomes extremely cold with a strong temperature inversion developing in the lower troposphere. The satellite detects low radiances from the area and inaccurately interprets these low values as cloud cover.

3.0 TEMPORAL VARIABILITY OF CLOUDS

Zonal averages of cloud cover can be misleading due to the averaging out of large longitudinal differences in cloud amounts. Therefore, in this chapter, I present global cloud analyses in horizontal projections where both longitudinal and latitudinal variations of cloud can be distinguished. I examine the analyses of the total and high cloud fields only, since the resulting fields of middle and low clouds as determined by satellite are not accurate due to the obstruction by high cloud. I have also deleted any discussion of data poleward of 63.5 degrees latitude.

3.1 Seasonal Mean

3.1.1 Total Cloud

The seasonal means for total cloud for the NH summer and winter seasons are shown in Figures 3.1 and 3.2, respectively. A prominent feature emerging in both seasons is the ITCZ. During the NH summer, the ITCZ is represented by a longitudinally continuous band of maximum amount of total cloud in the equatorial region of the globe lying predominantly in the NH. The intense convective activity of the ITCZ over southeast Asia during the NH summer is evident from the extensive cloud cover associated with it. When the ITCZ shifts southward during the NH winter, it is no longer shown to be a continuous band of cloud along the equatorial region of the globe. It is disrupted by the massive SH subtropical anticyclones which, at times, move into the tropical latitudes. This is especially true over the large Pacific Ocean. However, the intensity of the monsoon circulation aides in maintaining the continuous area of convection over the Indian Ocean.

The SH middle latitudes are represented by a zonal distribution of total cloud with little variation between seasons. During the NH winter, the location of the major cyclogenic regions,the Icelandic Low and Aleutian Low, can be located by cloud maximums. During

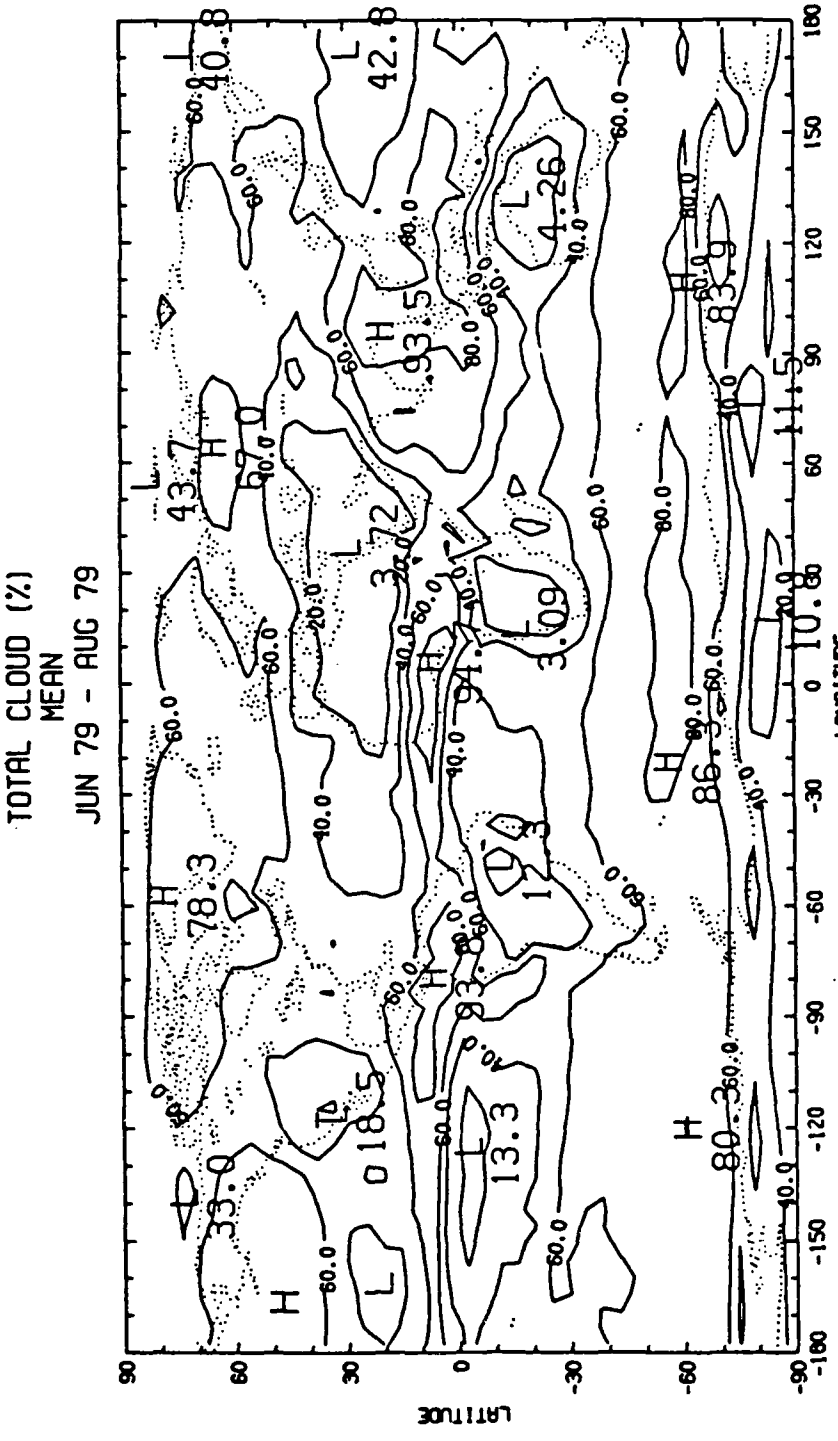

Figure 3.1 Global distribution of the total cloud mean for NH Summer.

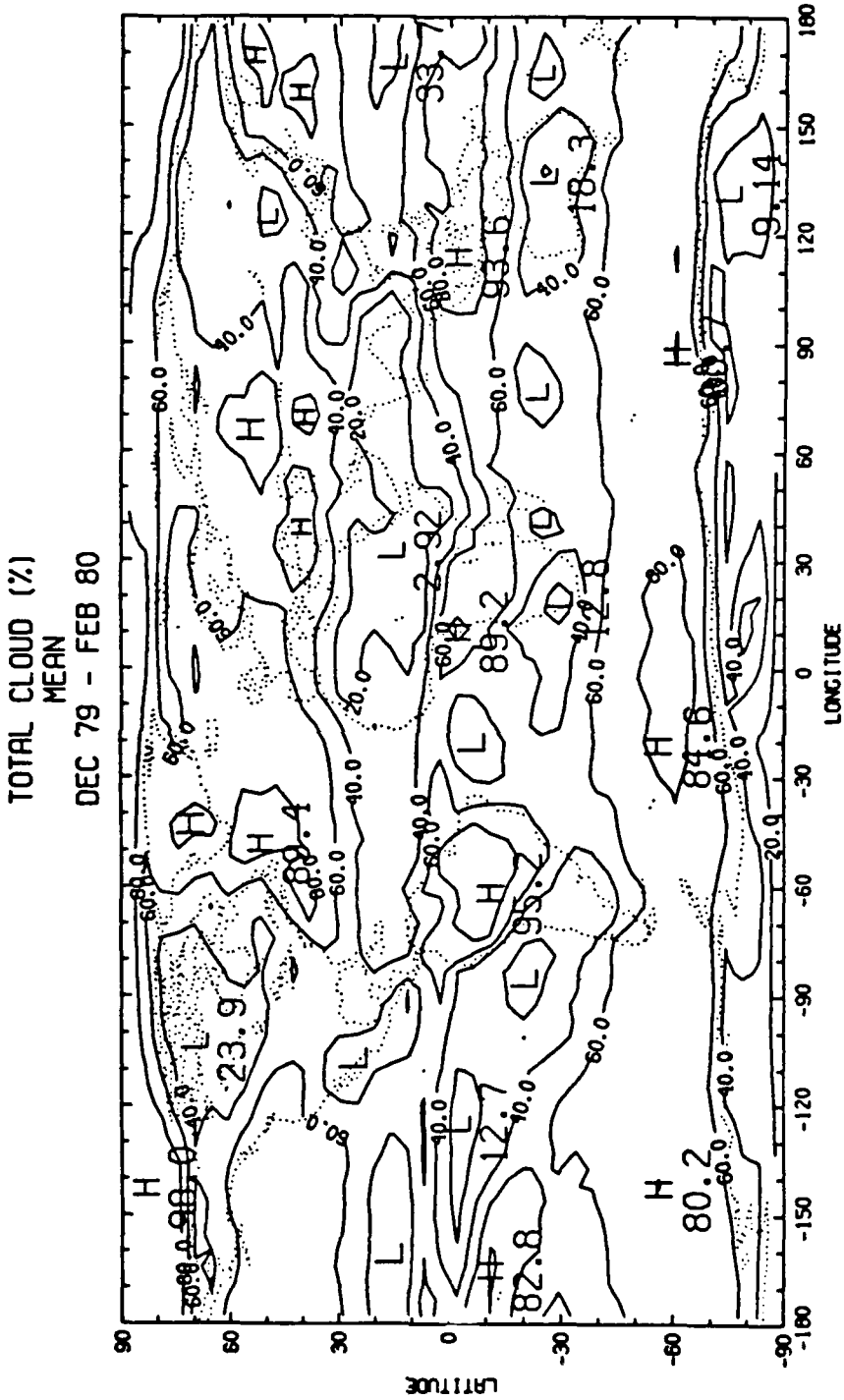

Figure 3.2 Global distribution of the total cloud mean for NH Winter.

the summer, the northerly retreat of these cloud areas is evident, especially for the Icelandic Low where there is also a significant decrease in cloud amount during the summer.

The subtropical areas, which contain the global deserts as well as the large subtropical anticylones, are represented by regions of minimum cloud amounts. Both the deserts and oceanic anticylones rely on massive subsidence to balance the net energy for their atmosphere resulting in dry, cloud-free regions. In the NH, the northern boundry of the dry subtropics is eroded by the middle latitude cloudiness associated with the storm systems in the winter, and the southern boundry is eroded by the ITCZ cloudiness in the summer. On the other hand, the subtropical cloud-free regions of the SH are altered mostly by the ITCZ on its equatorward side.

3.1.2 High Cloud

Figures 3.3 and 3.4 show the horizontal projection of high cloud over the globe for the NH summer and winter, respectively. Again, a very distinguishable feature is the location of the ITCZ. A strong gradient of high cloud is evident between the dry subtropics and the convective regions of the ITCZ. As noted in previous sections, the intensity of the convection is the cause for such an extensive amount of high cloud over the ITCZ. As the ITCZ shifts from the NH to the SH, there is a decrease in cloud amount as was observed for the total cloud.

The middle latitudes of the NH show no well developed maximum or minimum centers of high cloud during the summmer, but there is a relative minimum over the eastern Pacific extending over the western U.S. and over the eastern Atlantic extending over the western portion of he Eurasian continent. But by winter, the high cloud associated with the winter storm tracks becomes more evident. The areas of the Aleutian and Icelandic lows are well defined by maximum centers of high cloud. During the SH winter, the SH middle latitudes are characterized predominantly by a zonal structure of high cloud. A region of maximum high cloud located at about 35°S and between 110°W to 140°W represents a middle latitude storm track. By summer, the zonal structure is disrupted as the high cloud amount decreases and the dry subtropical anticyclones build into the middle latitudes.

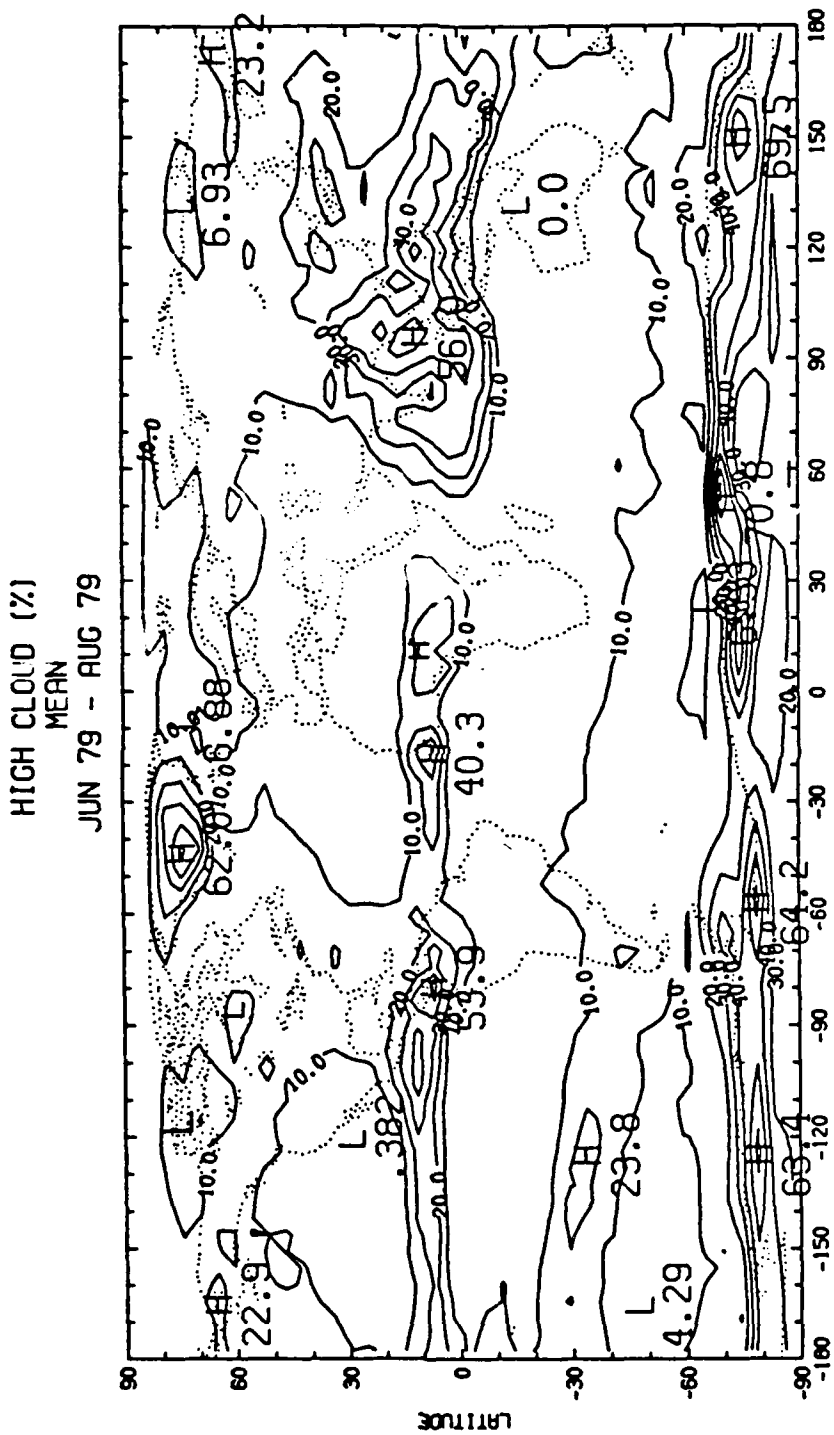

Figure 3.3 Global distribution of the high cloud mean for NH Summer.

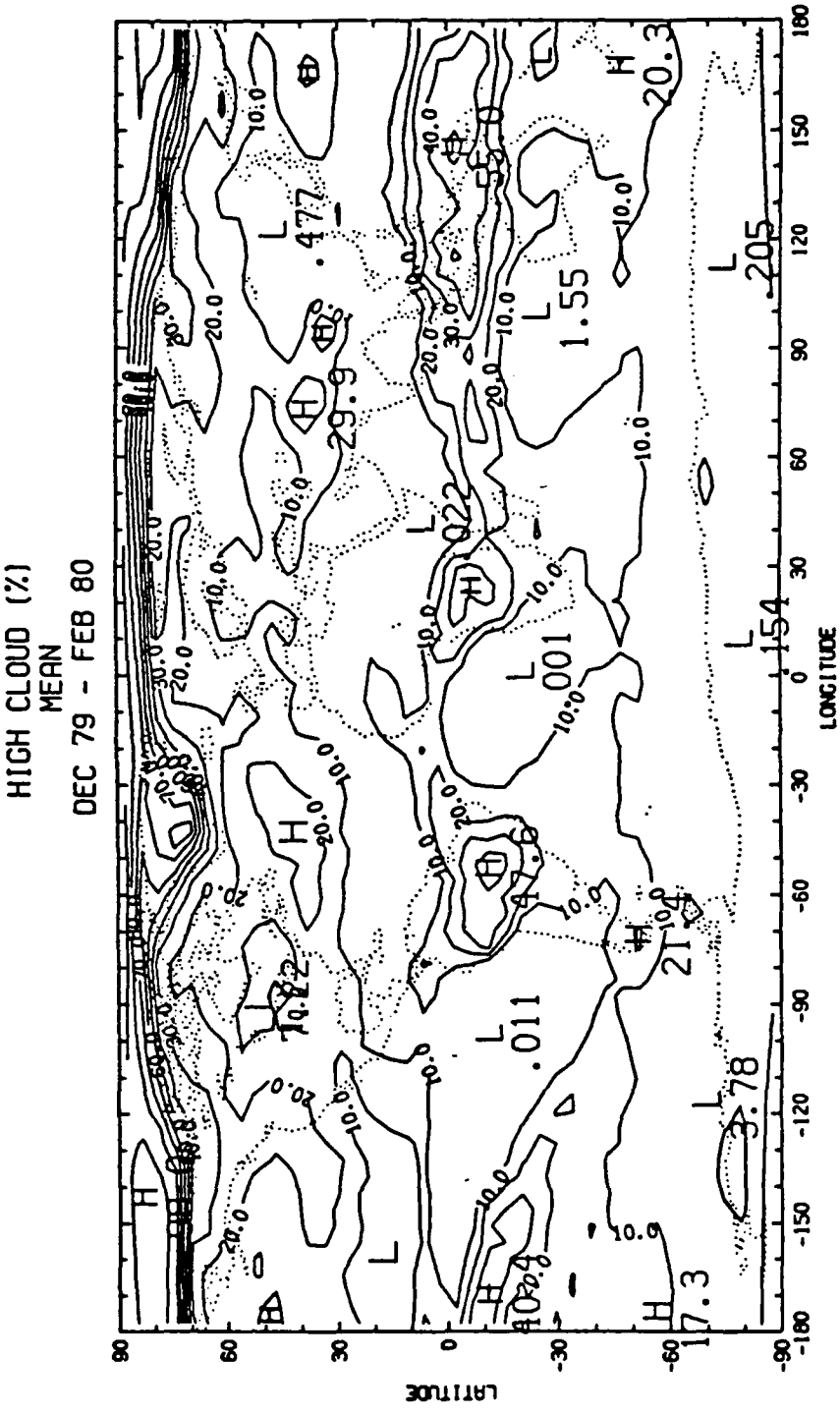

Figure 3.4 Global distribution of the high cloud mean for NH Winter.

3.2 Seasonal Standard Deviation

3.2.1 Total Cloud

During both the summer and winter seasons, the standard deviation fields of total cloud are not well defined for most regions as depicted in Figures 3.5 and 3.6. It is easier to interpret these fields by first examining regression analyses between the mean and standard deviation fields.

Figures 3.7 and 3.8 show the regression analyses of the mean and standard deviation fields for the winter and summer seasons, respectively. It can be seen that for small amounts of cloud cover, the standard deviation is small meaning regions over the globe with little cloud cover tend to remain cloud free. Areas with very large amounts of cloud cover are also characterized by a small standard deviation suggesting that cloudy regions are inclined to stay cloudy for the duration of the season. The areas characterized by intermediate cloud amounts depict a large standard deviation of cloud. These regions lie predominantly between the maximum and minimum centers of cloud cover where there is a strong gradient of cloud. Because of this gradient, these regions can experience a large fluctuation in its cloud cover during the course of a season as the cloudy and cloud-free regions go through small variations in space during the season. These regions of high standard deviation can be classified as cloud transition zones.

Examination of Figures 3.6 and 3.7, show that the desert regions over the African continent and the SH subtropical regions which are characterized by a small amount of cloud is also characterized by a small standard deviation of cloud cover. Areas where the mean cloud cover is large, such as the Aleutian and Icelandic Lows and the extreme centers of the ITCZ zones, are also characterized by a minimum standard deviation.

Regions of relative maximum standard deviation for total cloud are not as widespread as the minimum centers, but as discussed above, they exist in areas separating maximum cloud centers from minimum centers. The most predominant regions are near the ITCZ over Peru, Chile and northwest India.

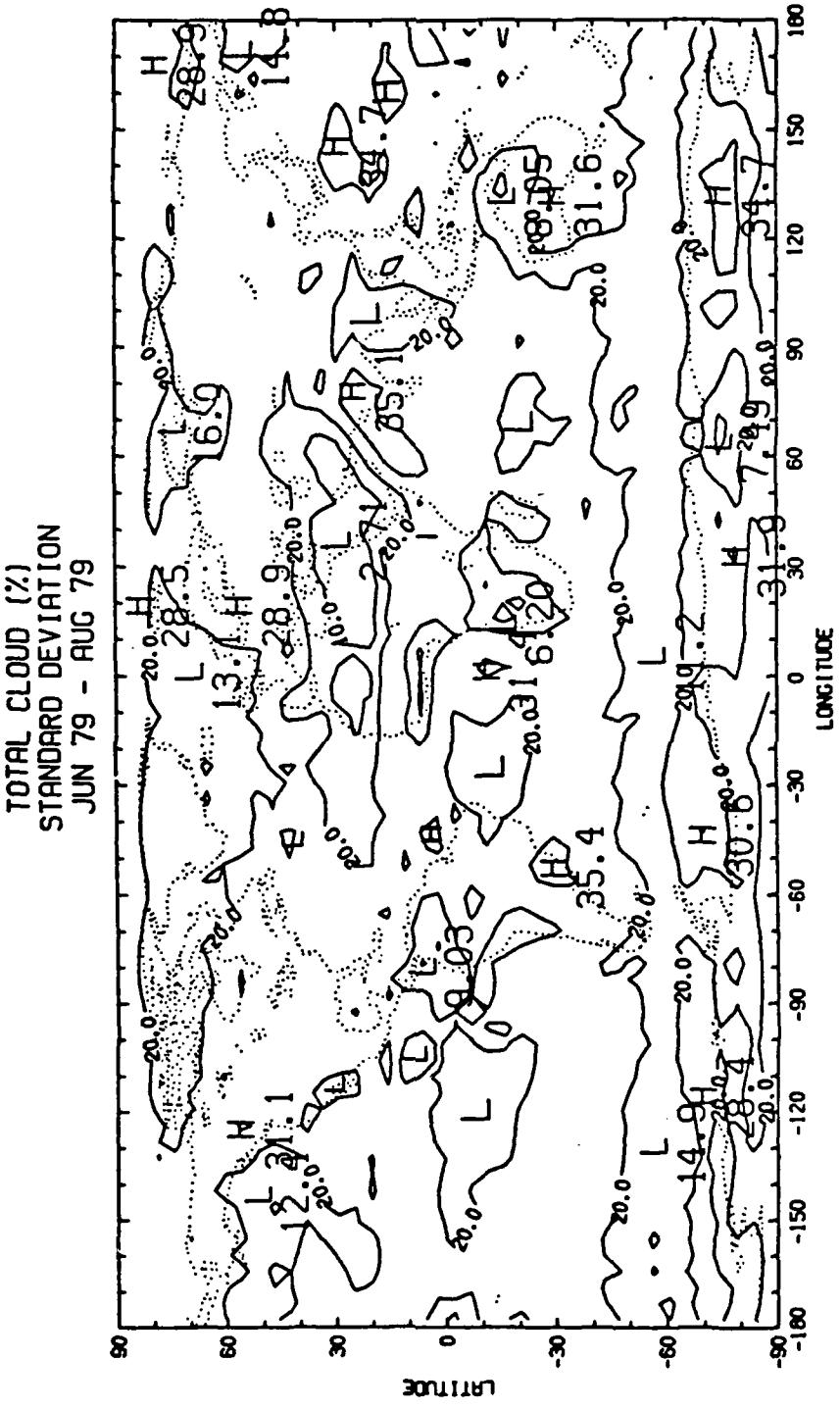

Figure 3.5 Global distribution of the total cloud standard deviation for NH Summer.

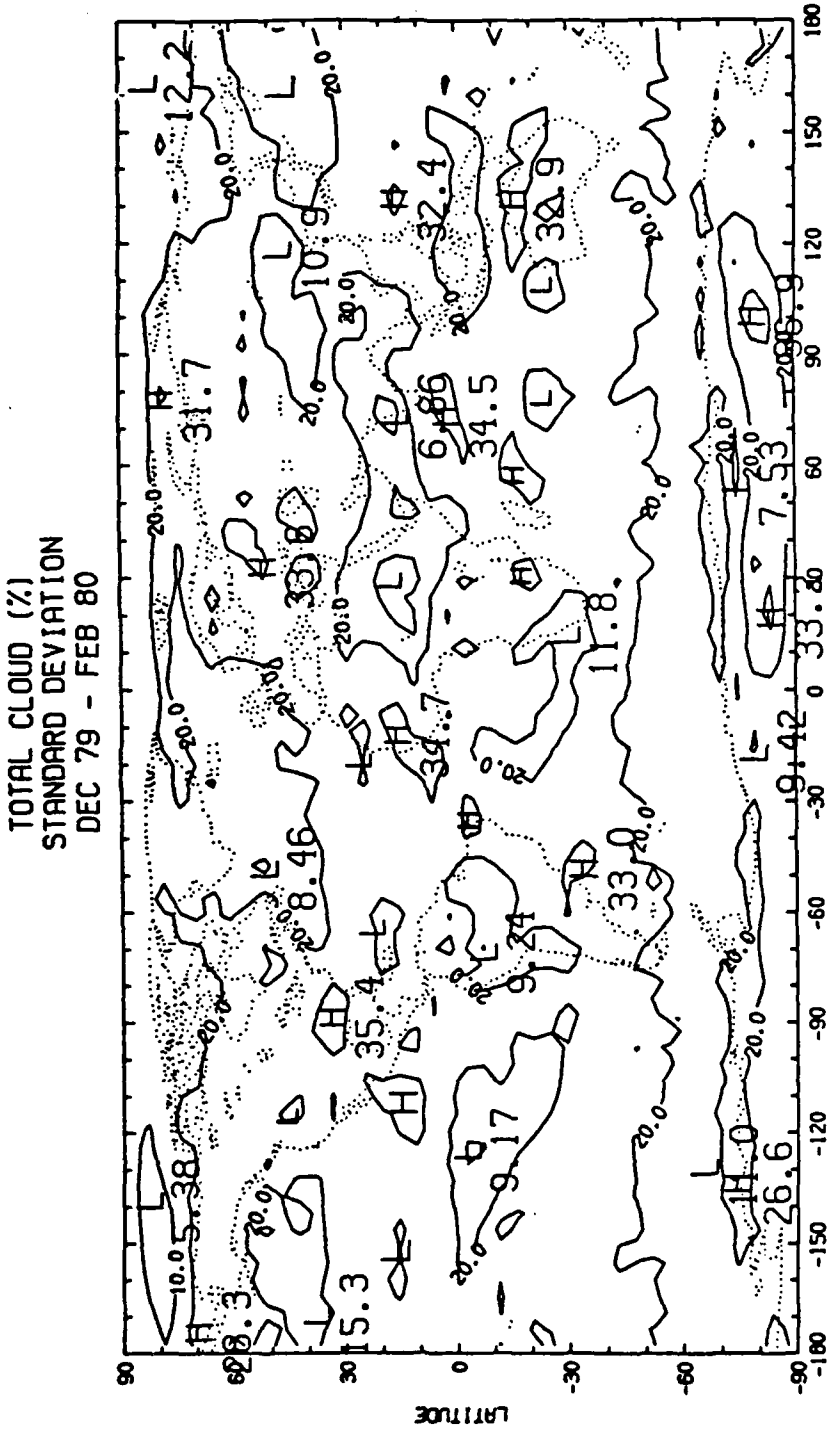

Figure 3.6 Global distribution of the total cloud standard deviation for NH Winter.

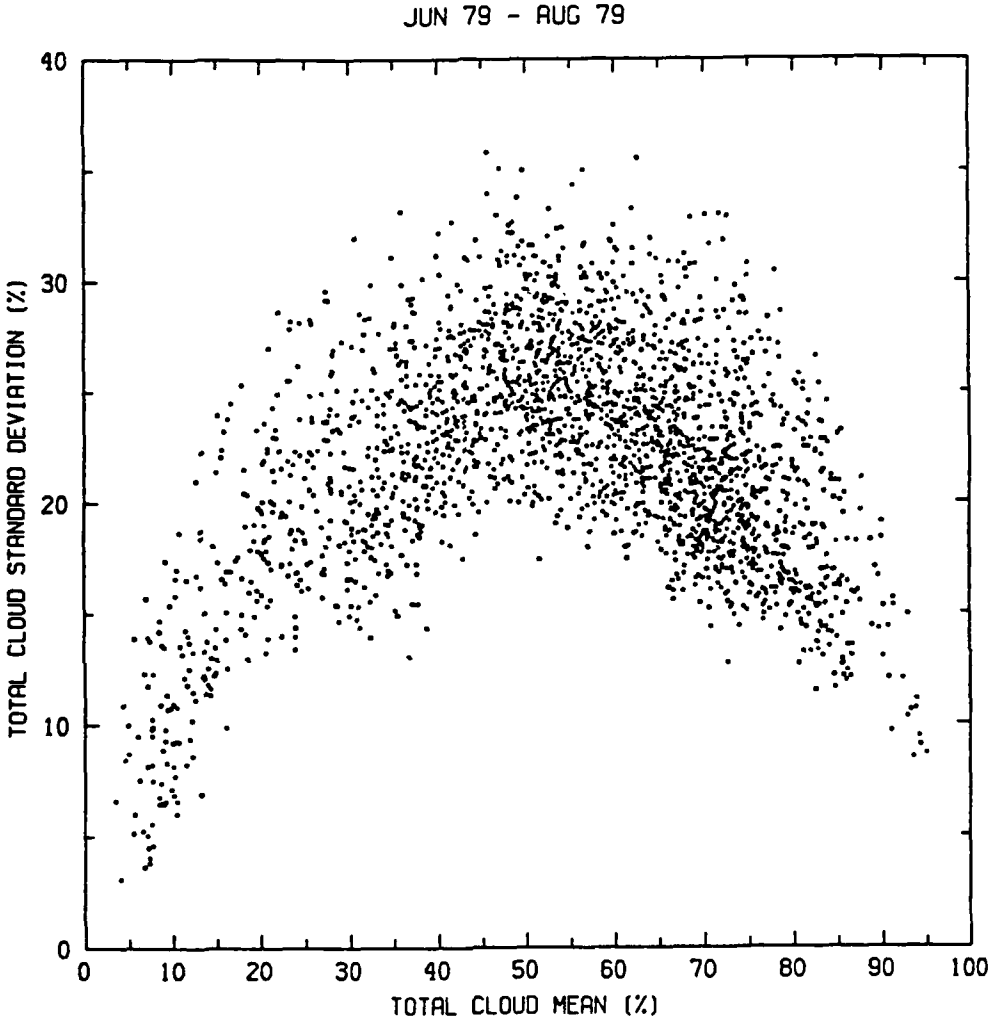

Figure 3.7 Regression analysis of total cloud mean vs. total cloud standard deviation for NH Summer.

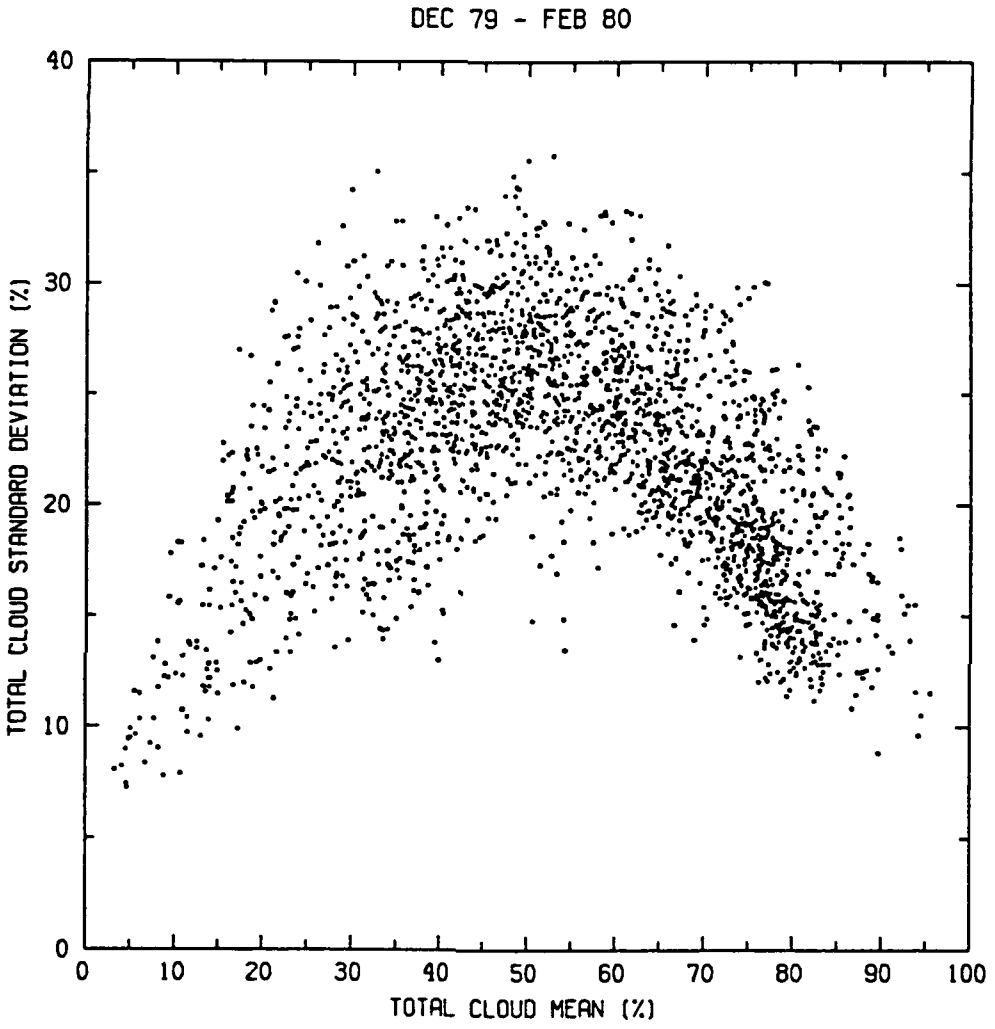

Figure 3.8 Regression analysis of total cloud mean vs. total cloud standard deviation for NH Winter.

3.2.2 High Cloud

Even though the standard deviation field of high cloud for summer and winter (Figures 3.9 and 3.10) is relatively easy to interpret, an initial examination of the regression analyses between the mean and standard deviation fields, Figures 3.11 and 3.12, is helpful. The analyses indicate that a strong positive correlation exists between the mean amount of high cloud and its standard deviation for both winter and summer seasons. As with the total cloud, regions of small high cloud amounts depict little variation in the cloud amount. But as the amount of high cloud increases, the standard deviation increases almost linearly at first, becoming assymtotic for greater amounts of cloud. Large amounts of high cloud tend to be associated with either convective regions such as the ITCZ or the advective storm tracks of the middle latitudes. The daily variability of convective and advective processes leads to a large standard deviation of high cloud over these areas during a season. The variaion of high cloud can be used for study of precipitation patterns over convective regions. Recall that the standard deviation of the total cloud is small for these regions. A change in the ratio of the high cloud amount to total cloud amount could be used to define an index of the onset of convective activity.

An examination of Figures 3.9 and 3.10 reveals that the location of the centers of maximum standard deviation for high cloud correlates exactly with the centers of maximum mean of high cloud. Most noticable are the convective ITCZ regions. Also, the centers of minimum standard deviation lie directly over the centers of maximum high cloud amount being most evident over the deserts and the subtropical anticyclones. Note that there is a slight maximum along the the southeatern coasts of South America, Australia, and Africa during the SH winter. These centers depict middle latitude storm tracks where, even though in the seasonal mean there is no significantly large amount of high cloud, the variability of high cloud is large.

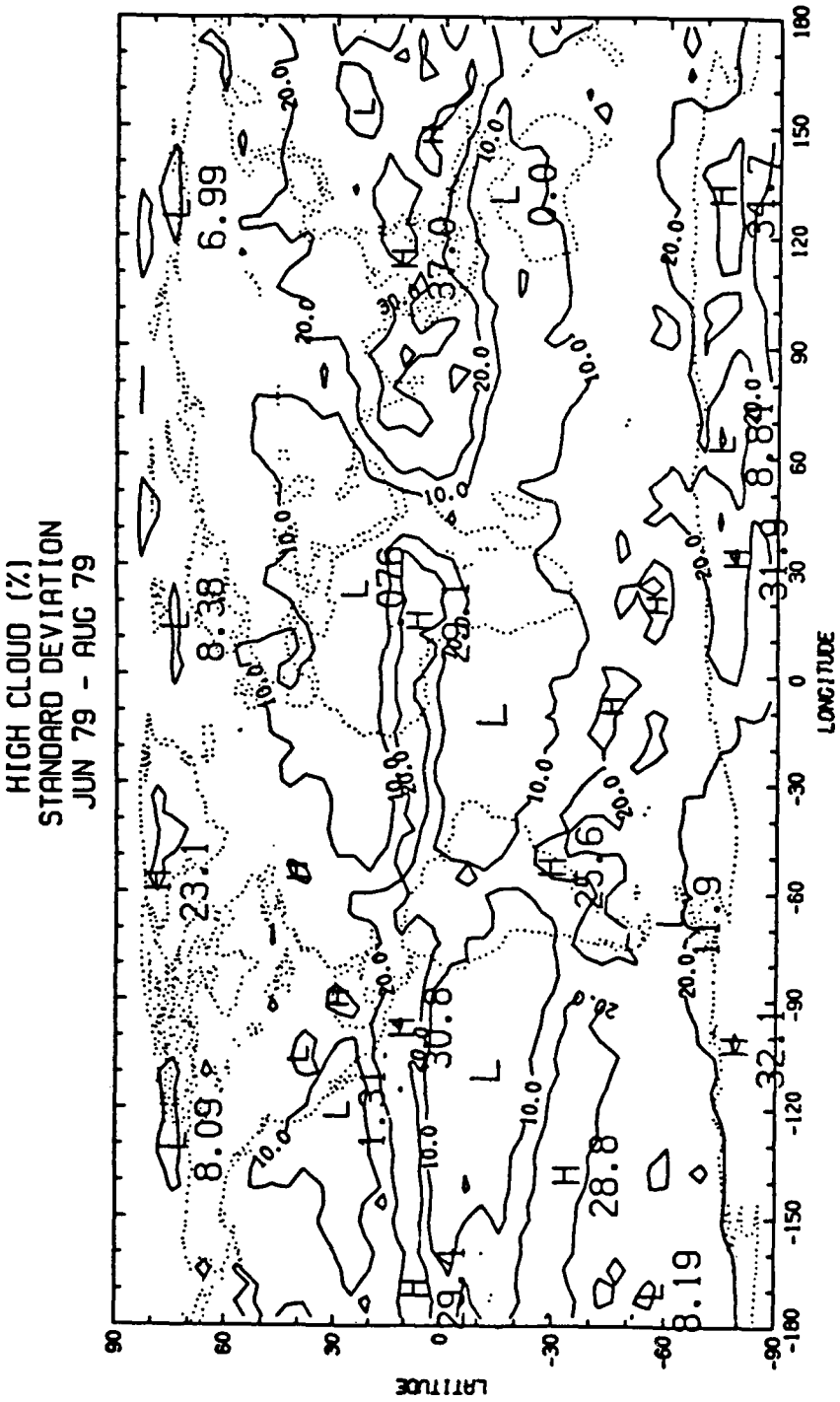

Figure 3.9 Global distribution of high cloud standard deviation for NH Summer.

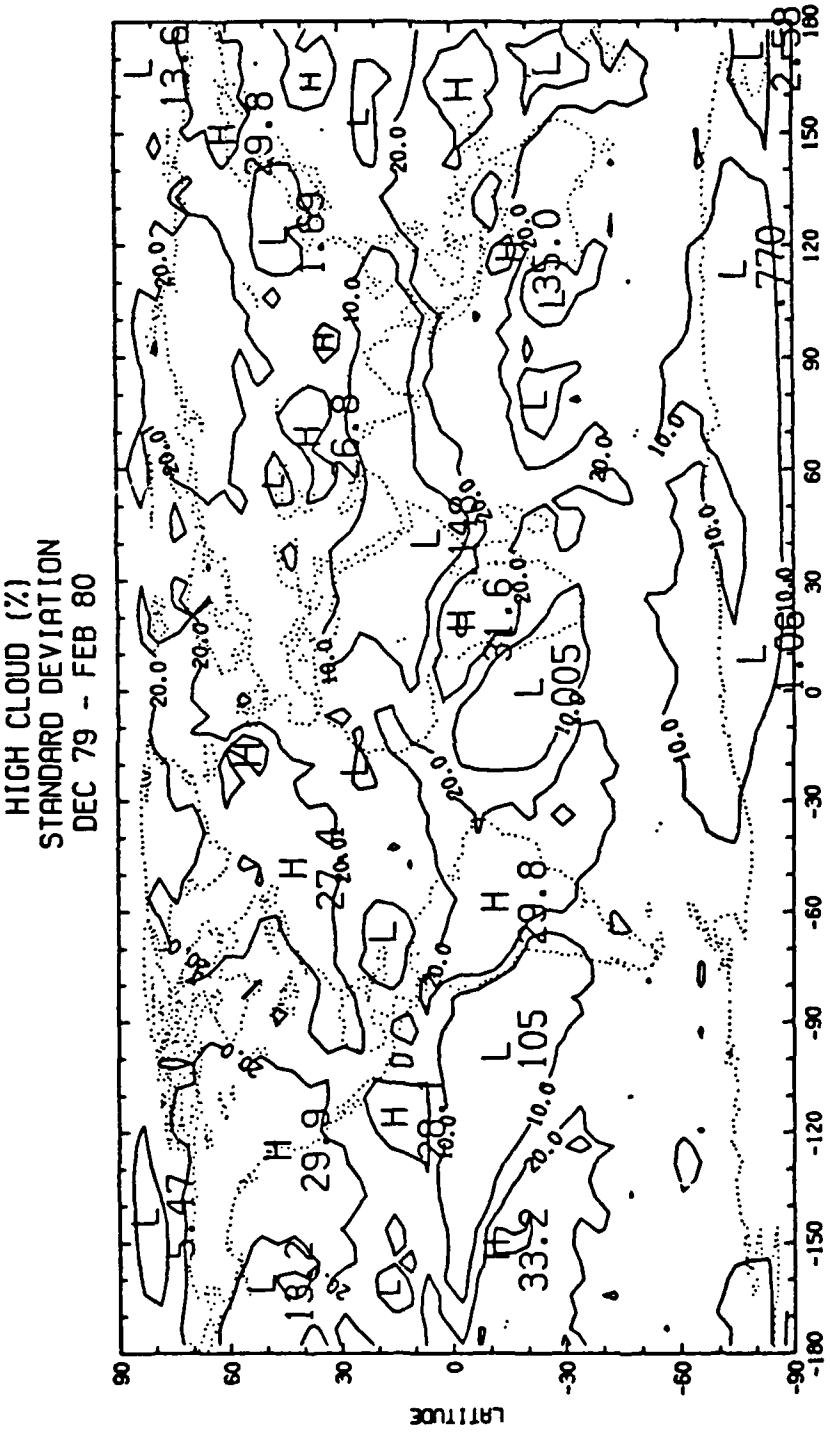

Figure 3.10 Global distribution of high cloud standard deviation for NH Winter.

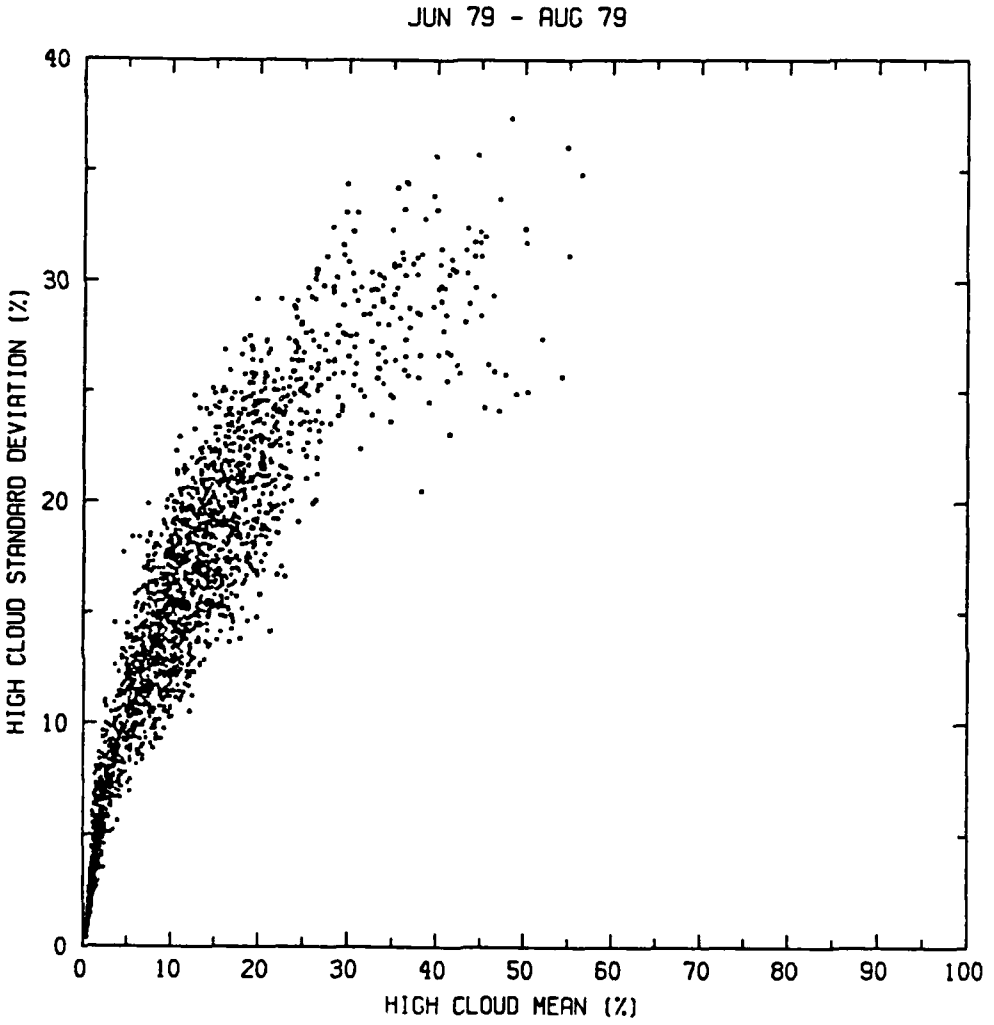

Figure 3.11 Regression analysis of high cloud mean vs. high cloud standard deviation for NH Summer.

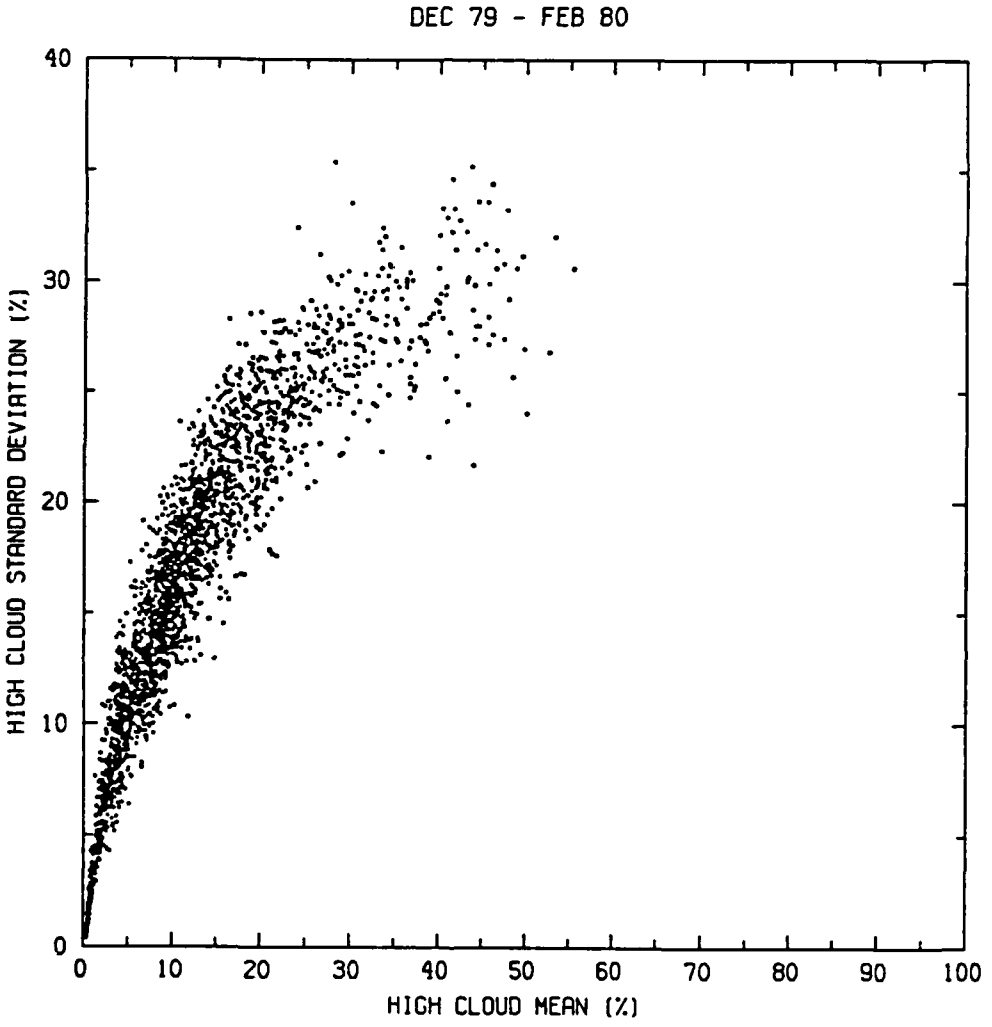

Figure 3.12 Regression analysis of high cloud mean vs. high cloud standard deviation for NH Winter.

4.0 TEMPORAL VARIABILITY OF IR

In this chapter, I will discuss the analyses of the seasonal means and standard deviations of IR for the summer and winter seasons analyses. The source of IR data used is from the narrow field of view sensor on the Earth Radiation Budget (ERB) instrument on board the NIMBUS 7 satellite. The data is stored on the MATRIX tapes in the same format used for the CMATRIX tapes. A description of the ERB instrumentation and data sets can be found in Jacobowitz *et al.* (1984) and Randel (1983). An analysis of the global IR can also be found in Smith and Vonder Haar (1988).

4.1 Seasonal Mean

Figures 4.1 and 4.2 represent the seasonal averages of the global IR for the NH summer and winter seasons, respectively. Examination of these mean fields reveals that the position of the major features correspond to the major features of the mean high cloud with centers of maximum IR overlying centers of minimum high cloud and vice versa.

The ITCZ region which is characterized by a maximum of high cloud is also defined by a band of minimum IR. The seasonal shift of the ITCZ is evident in the IR as a broad band of minimum IR situated over southeast Asia and India during the NH summer shifting to a narrower band of minimum IR positioned over Indonesia during the NH winter. Note that most of the centers of the minimum IR values are located over land corresponding to the high cloud maximum location. It is the increase heating of the land surfaces producing high cloud shields.

The subtropics, characterized by minimum high cloud cover, are also defined by maximum amount of IR flux. The larger values of IR over the nothern African deserts in the summer are due to the higher surface temperatures during this season. The SH summer subtropical anticylones are well defined by large areas of maximum IR. The eastern sections

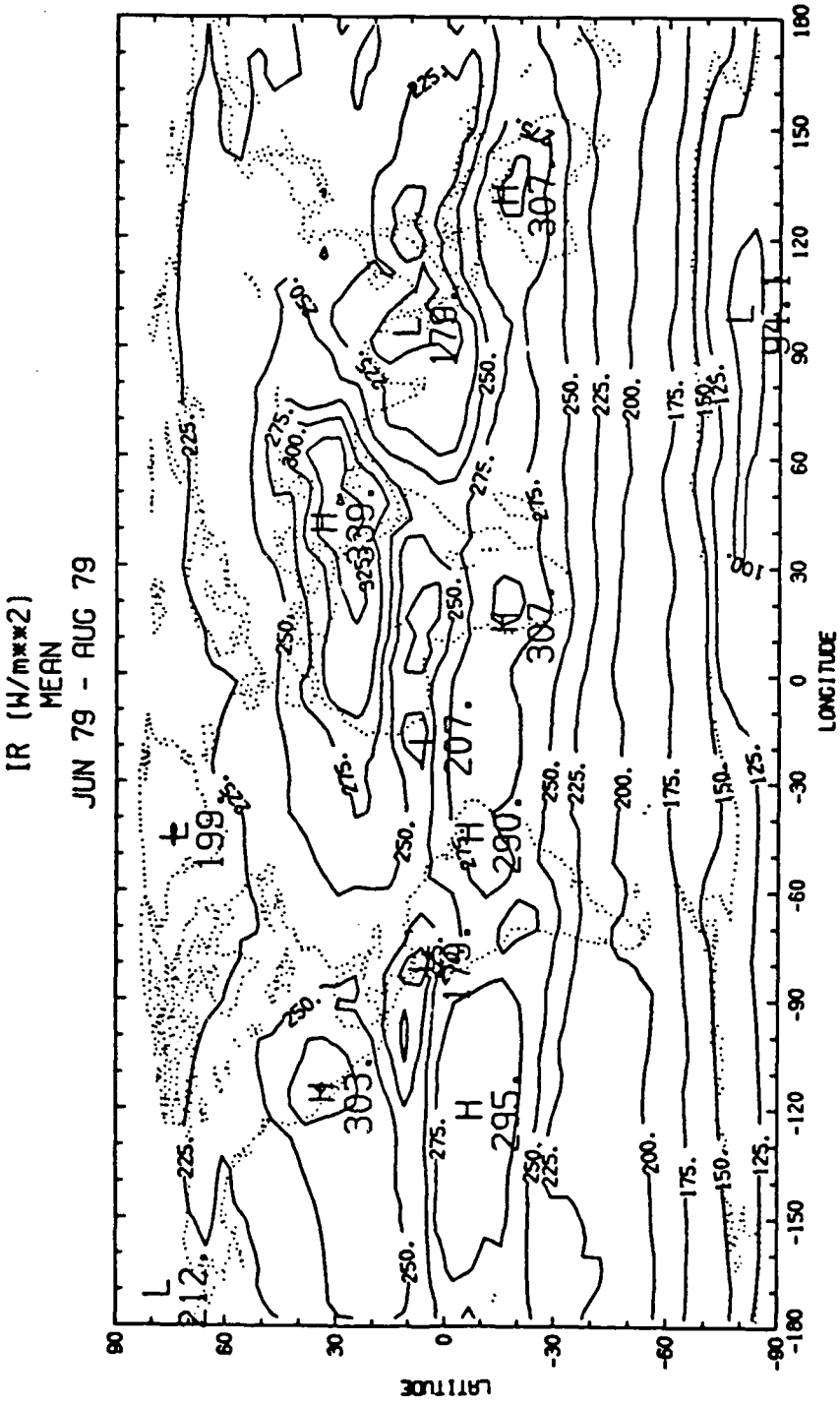

Figure 4.1 Global distribution of IR mean for NH Summer.

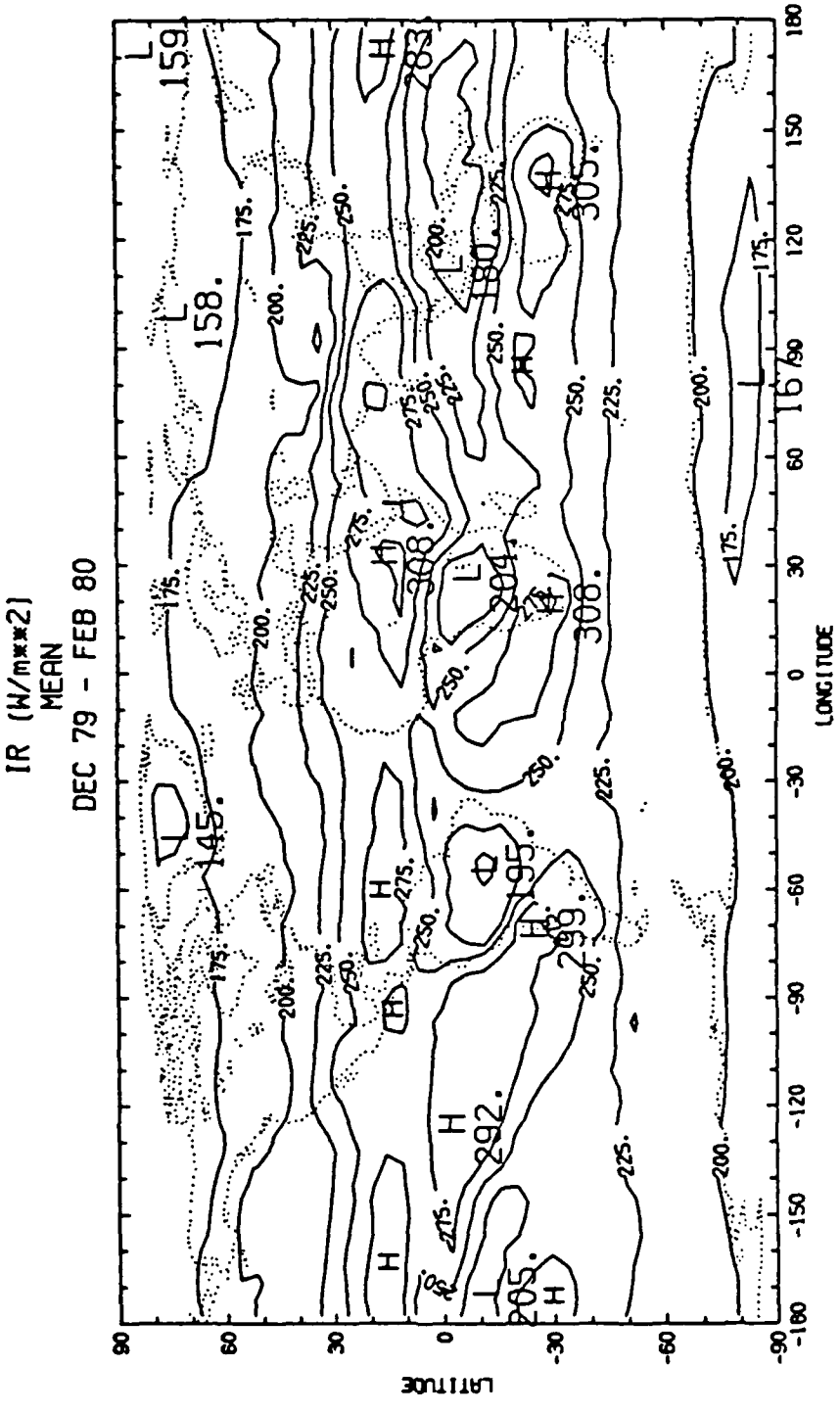

Figure 4.2 Global distribution of IR mean for NH Winter.

of the subtropical highs, characteried by persistent low level cloud, is shown to emit large values of IR.

The SH middle latitude belts, defined by a zonal structure of high cloud, are also represented by a zonal pattern of IR during the SH winter season. The IR pattern is a result of the north–south gradient of surface temperature within these latitudes. During the SH summer, the zonal pattern is still evident but is disrupted on the equatorward side by the maximum IR centers which have moved into the middle latitudes. The winter NH middle latitudes depict the same zonal pattern of IR with lower values to the north. This does not correlate well with the projection of high cloud over this area. The centers of maximum and minimum high cloud are only relatively large and small compared to the surrounding regions, i.e., a gradient is almost nonexistent.

An important observation of the mean IR fields is that the highest correlation between high cloud and IR emerges in the low latitudes. This is the region of intense solar heating resulting in strong convection with the associated high cloud shields and low fluxes of IR along the ITCZ. It is also the region of the dry, cloud-free regions of the deserts and subtropial anticyclones which exhibit large fluxes of IR to space.

4.2 Seasonal Standard Deviation

A glance at Figures 4.3 and 4.4 indicates that the standard deviation fields of the IR are rather nondescript over most regions of the globe and show little correlation to the mean IR fields. The most noticeable features are the low values of standard deviation defining the subtropical anticyclones of the SH. The strong subsidence and stability of the subtropics produces a persistent, relatively cloud-free atmosphere (low high cloud standard deviation) over regions through an entire season corresponding to the low IR standard deviation. Even though small fluxes of IR are characteristic of the ITCZ in the seasonal mean, the standard deviation of IR is large. This is consistent with the large variation of high cloud over the area.

In the middle latitudes of the SH winter, centers of maximum standard deviation emerge along the southeast coasts of South America and Africa even though in the mean, the IR was represented by a smooth zonal structure. This variation between the mean and standard

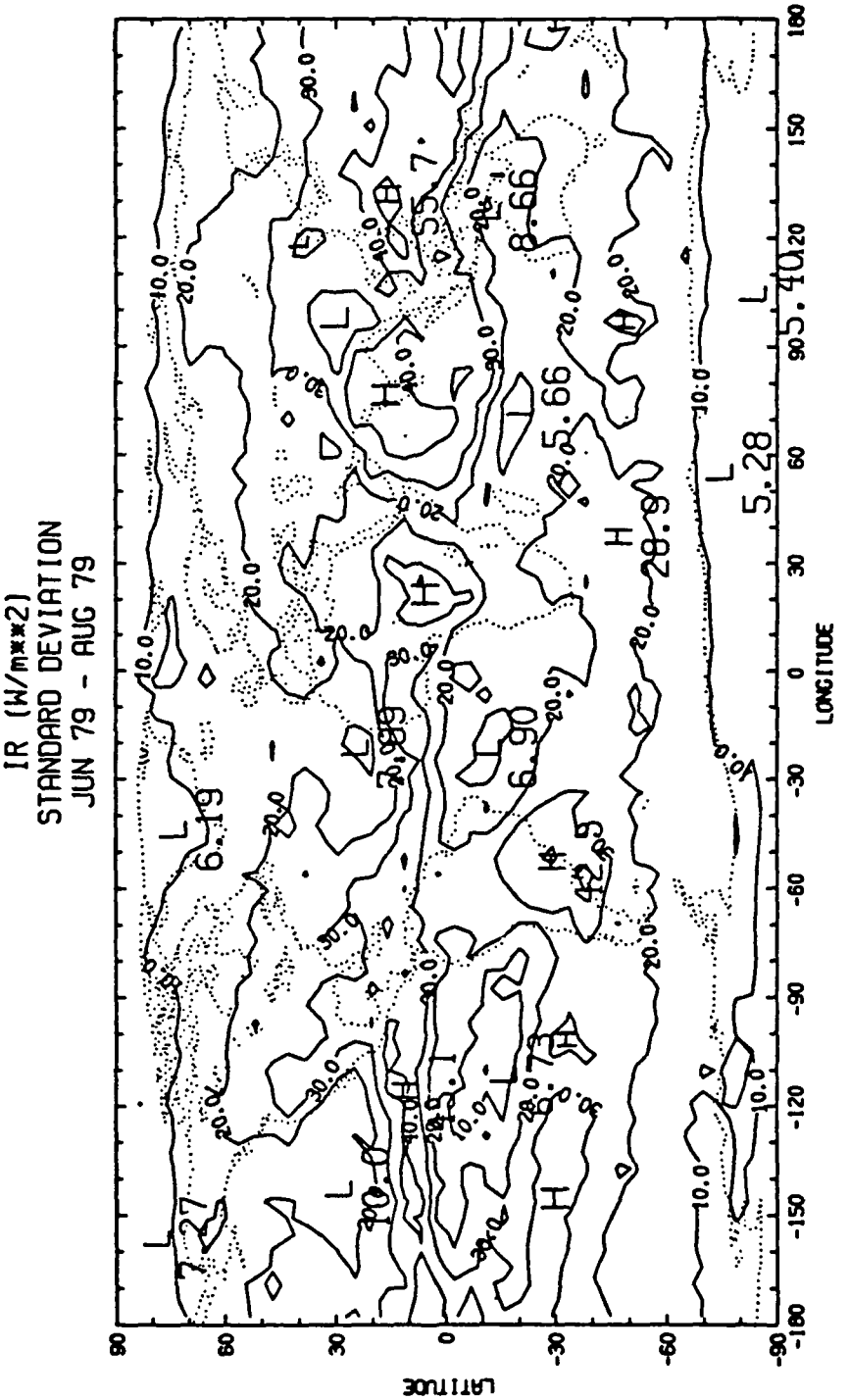

Figure 4.3 Global distribution of IR standard deviation for NH Summer.

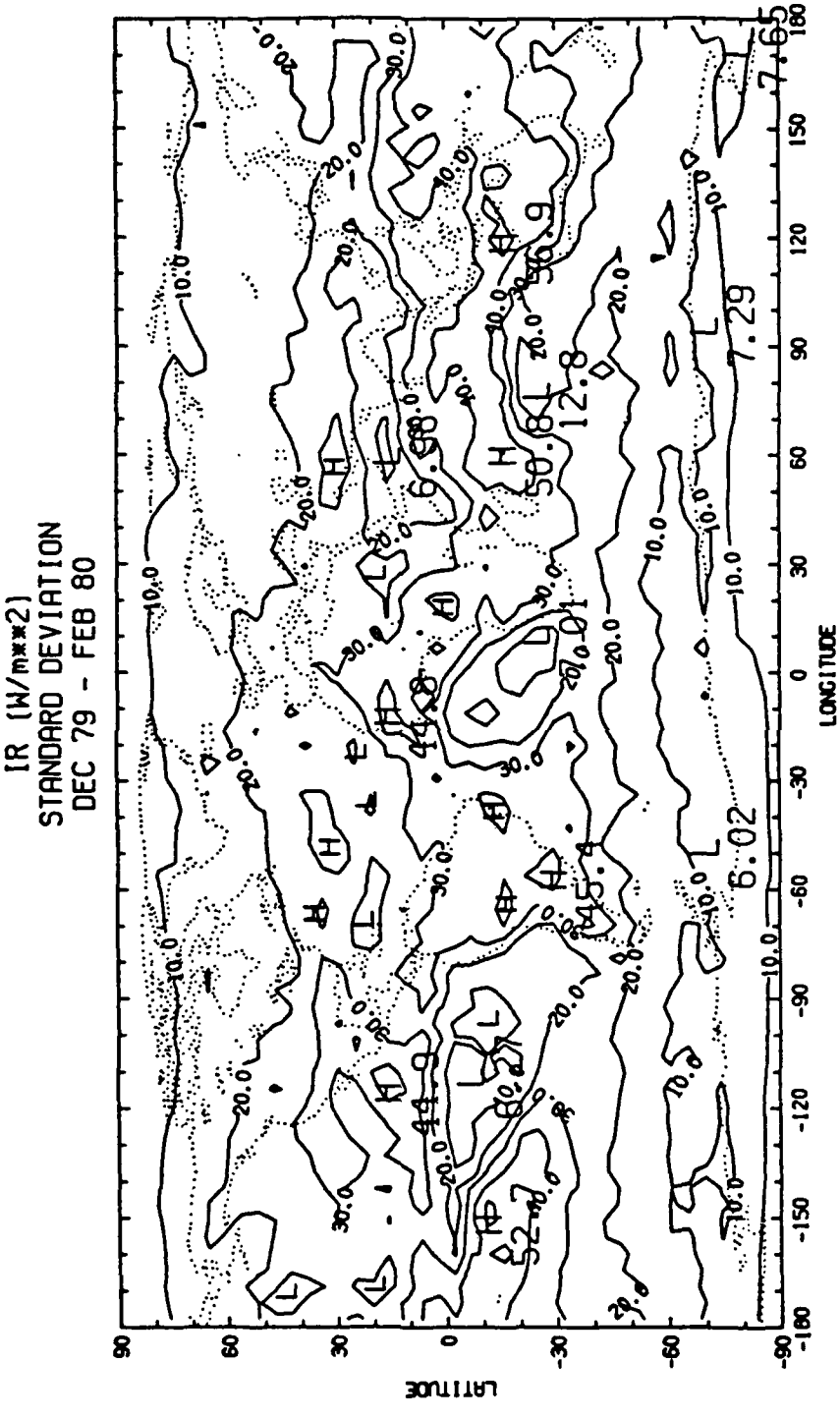

Figure 4.4 Global distribution of IR standard deviation for NH Winter.

deviation fields was also evident in high cloud over this area. In the NH winter middle latitudes there is little organization of the standard deviation field. However, along the storm tracks in the U.S. there is a slight indication of high variability of IR coinciding with the variability in high cloud.

5.0 HIGH CLOUD–LONGWAVE RADIATION INTERACTION

The ultimate purpose of this chapter is to present a correlation between high cloud and longwave radiative flux from the earth–atmosphere system. However, before analyzing the results of this study, it is necessary to understand the transfer of longwave radiation through a clear and cloudy atmosphere.

5.1 Theory

5.1.1 Longwave Radiation in a Clear Sky

The longwave radiation emitted from the earth–atmosphere system is a function of the temperature of the system and is experessed by the the Stefan-Boltzmann law

$$\sigma T_g^4$$

where σ is the Stefan-Boltzmann constant and T_g is the surface temperature. Longwave radiation from the earth's surface is transmitted directly to space through the atmospheric window, 8 to 14 μm range. However, there are interferences encountered by longwave radiation as it passes through the atmosphere. About 70% of the IR from the surface is absorbed by gases in the clear atmosphere, mostly by water vapor and carbon dioxide. Kirchoff's law ($\epsilon_\lambda = a_\lambda$) states that bodies which absorb radiation (a_λ) at a given wavelength also emit radiation (ϵ_λ) at that wavelength. So the atmospheric gases which absorb radiation also emit radiation at the same wavelength back to the surface and up to space. The downward emission is absorbed by the surface. The value of this emission is a function of the atmospheric temperature and water vapor content but can be expressed to a first approximation as a function of surface temperature by

$$\epsilon_1 \sigma T_g^4$$

which is an emission at wavelengths outside the atmospheric window and where ϵ_1 is the

flux emissivity of the atmosphere as viewed from the ground. Therefore, the amount of radiation transmitted directly to space can be expressed by

$$(1-\epsilon_1)\sigma T_g^4$$

which is radiation transmitted through the atmospheric window.

Evaluation of the amount of radiation emitted to space from the atmosphere is complicated due to variations in atmospheric temperature and gases for the various levels of the atmosphere. However, it can be simplified when considering that with the depletion of atmospheric gases with increased altitudes, there is a larger percentage of emitted atmospheric radiation reaching space from these higher levels of the atmosphere. In reality, each layer of the atmosphere radiates at its own temperature, but for simplification it can be assumed that radiative emission from the atmosphere is directly related to surface black body emission expressed by

$$\hat{G}\sigma T_g^4$$

where $\hat{G}$ is a proportionality constant between atmospheric longwave emission to space and surface black body emission. Finally, radiation emitted to space from a clear sky is expressed as

$$\hat{G}\sigma T_g^4 + (1-\epsilon_1)\sigma T_g^4$$

5.1.2 Longwave Radiation in a Cloudy Sky

In a cloudy sky, the longwave radiation emitted by the surface and by the atmosphere beneath the clouds is absorbed by the clouds. Clouds and the atmosphere below emit radiation back to the earth's surface. The radiation from the clouds, dependent on their black-body temperature, is transmitted mostly through the atmospheric window. Assuming an average cloud temperature, the amount of IR returned to the surface from the cloud and underlying atmosphere is

$$(1-\epsilon_1)\hat{\theta}\hat{f}\sigma T_g^4$$

where $\hat{\theta}$ is the fractional cloud cover and $\hat{f}$ is the ratio of cloud black body emission to surface black body emission. The clouds and atmospheric gases above clouds contribute

to the longwave radiation emitted to space from the atmophere above the clouds and is represented by the equation

$$\hat{\theta}(1-\epsilon_2)\hat{f}\sigma T_g^4$$

where ϵ_2 is the flux emissivity of the atmosphere above the average cloud level. And the total amount of longwave radiation emitted to space from the earth–atmosphere system is

$$(1-\hat{\theta})\,\sigma T_g^4[\hat{G}+(1-\epsilon_1)]+\hat{\theta}\,(1-\epsilon_2)\hat{f}\sigma T_g^4$$

The cooling of the earth–atmosphere system is not only dependent on the presence of clouds but also on the elevation of the cloud layer. Low level clouds, which have approximately the same radiative temperature as the surface, of the earth, will experience virtually no warming on their bottom sides from the earth's surface. However, from the tops of low level clouds, there is a large loss of IR to space due to the high temperature of the cloud tops. The interaction with high clouds is nearly opposite. Since high cloud has a low radiative temperature, the top of the cloud emits very little radiation to space but experiences a large warming from the earth and atmosphere below ("greenhouse effect"). The net effect is a low IR output to space in the presence of high clouds.

5.2 Regression Analyses

To relate IR response to the presence of high cloud, regression analyses have been performed for the globe, a regioanl area, and subregional areas. For the global and regional analyses, each data point represents a mean or a standard deviation value of IR and high cloud from a grid point measuring 4.5 degress latitude by 4.5 degrees longitude (3200 grid points cover the globe). The global analyses have been restricted to the area between 63.5°N to 63.5°S latitude, and the regional analyses have been restricted to the area between 31.5°N to 31.5°S latitude. For the subregional analyses, each data point represents the daily IR and high cloud value for specific grid points.

5.2.1 Global Analyses

Figures 5.1 through 5.4 depict the regression analyses between mean and standard deviation fields of high cloud and IR for the summer and winter seasons. The expected negative

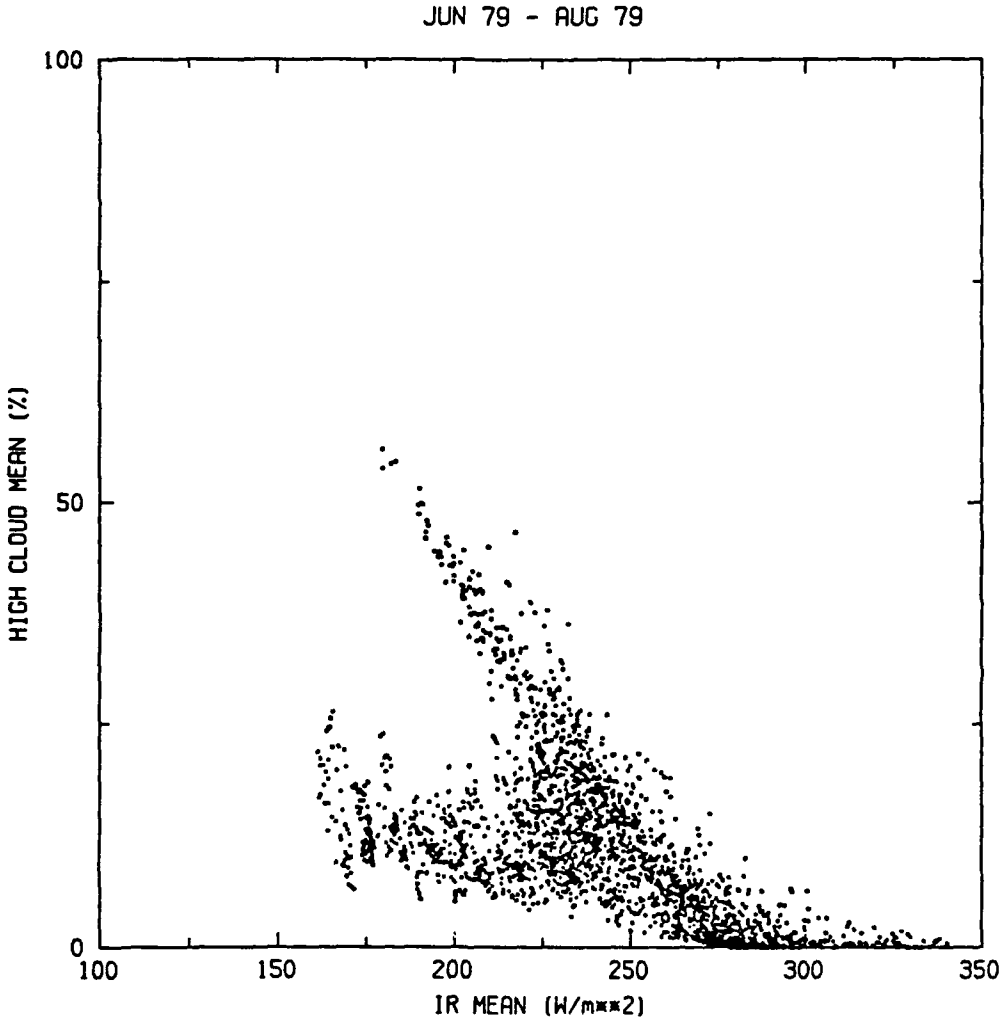

Figure 5.1 Regression analysis of IR mean vs. high cloud mean for NH Summer (63.5°N - 63.5°S).

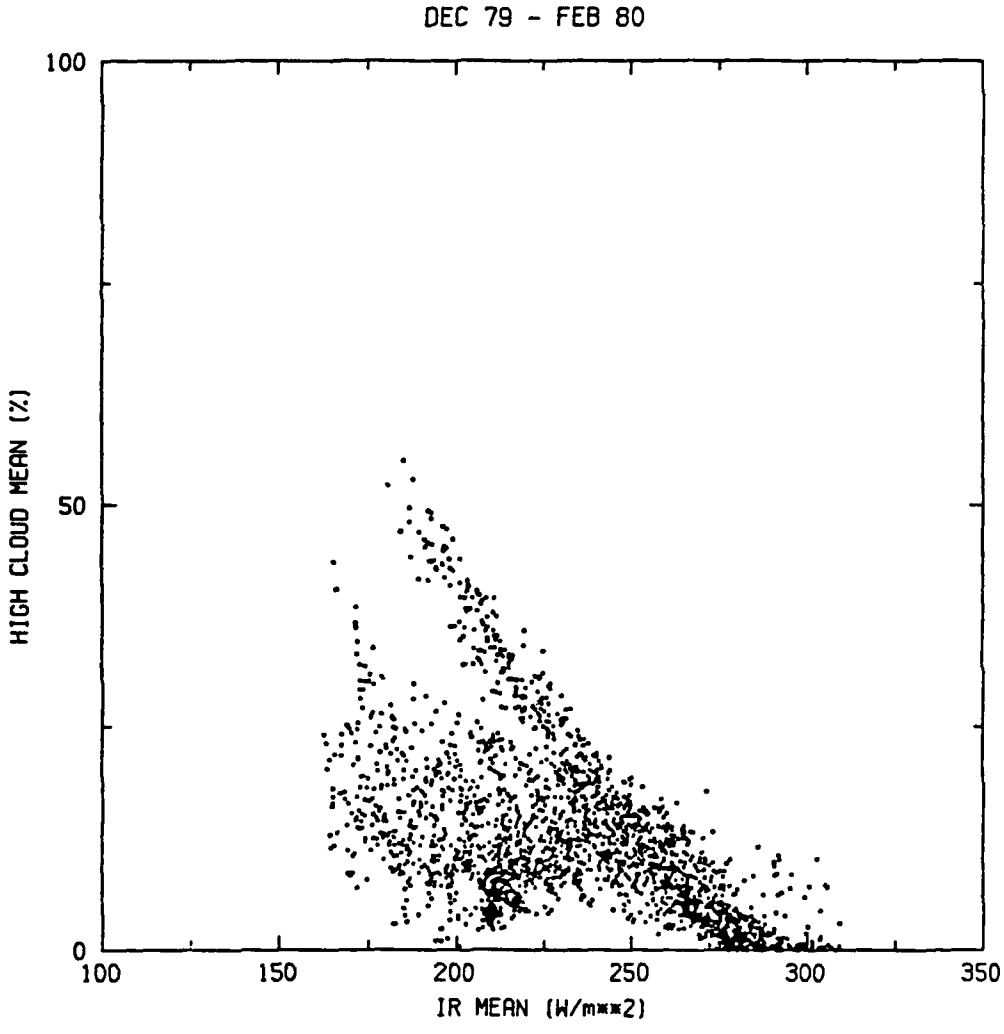

Figure 5.2 Regression analysis of IR mean vs. high cloud mean for NH Winter (63.5°N - 63.5°S).

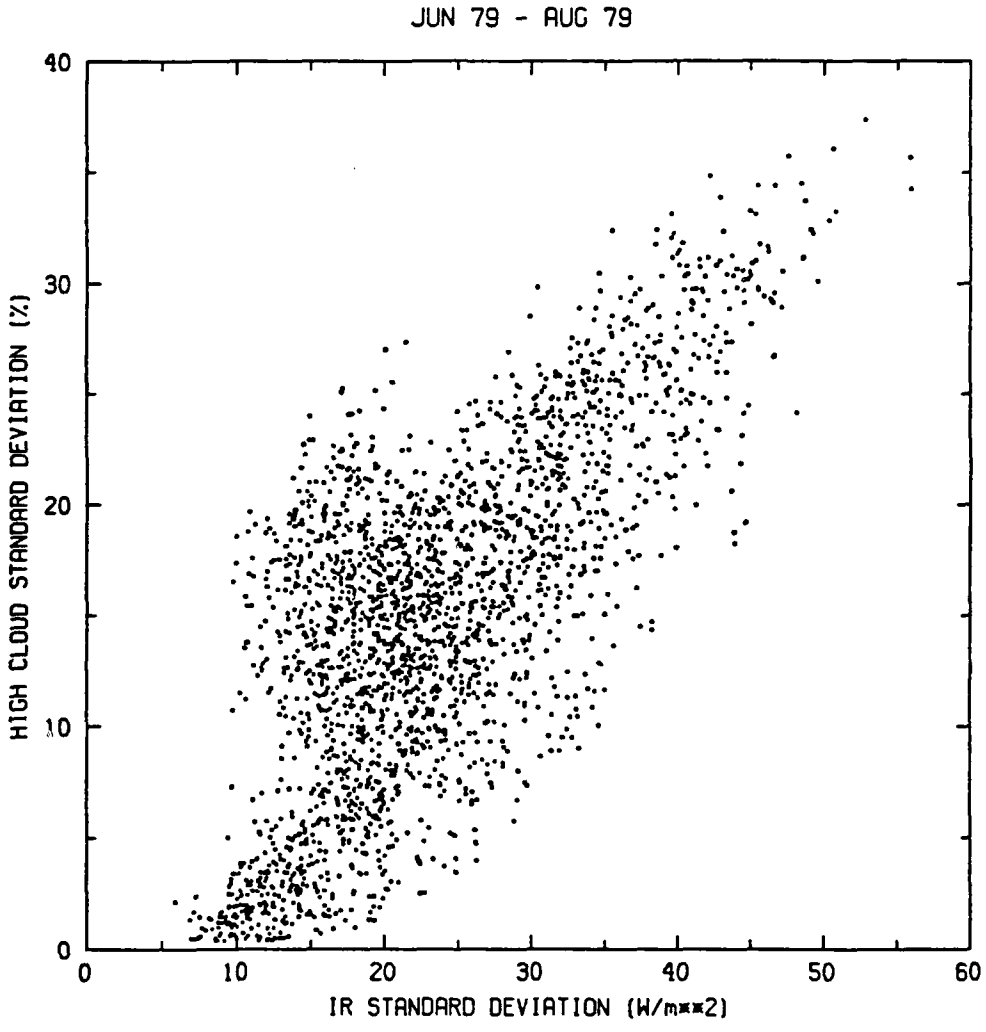

Figure 5.3 Regression analysis of IR standard deviation vs. high cloud standard deviation for NH Summer (63.5°N - 63.5°S).

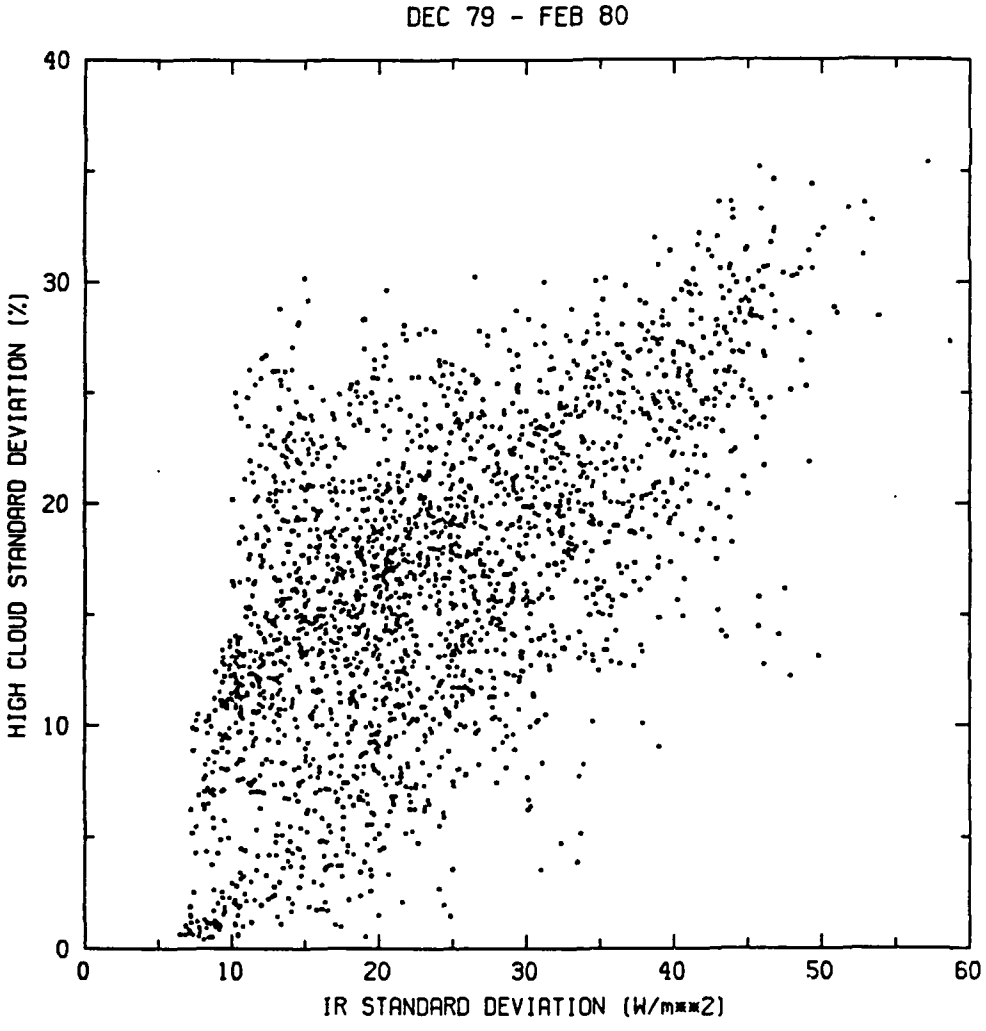

Figure 5.4 Regression analysis of IR standard deviation vs. high cloud standard deviation for NH Winter (63.5°N - 63.5°S).

correlation between the mean fields emerges in the graph for data points representing the low latitudes of the globe where there is a strong signal between high cloud and IR. Data points corresponding to large IR values and small cloud amount represent the subtropical anticyclones and desert regions. Values of small IR and large cloud depict the ITCZ regions where low values of radiation are emitted by the cold, high altitude cirrus shields.

The data points depicting low IR values associated with low amounts of cloud represent the middle latitudes. In the high latitudes, the emitted surface radiation is low due to low surface temperatures, so even with a small amount of high cloud, the IR fluxes are not large compared to the values measured in the lower latitudes. In the NH winter, there is a higher concentration of data points in this portion of the analysis due to the cold surface temperatures of the land mass. This feature is not as prominent for the SH winter where there is a small land to ocean ratio.

The analyses between the standard deviation fields depict a trend of positive correlation between high cloud and IR. Recall that areas with an abundant amount of high cloud are defined by a large variability of the cloud cover, and areas having a inappreciable amount of high cloud present a small variability of the cloud amount. For regions where there is a strong signal between IR and high cloud, the standard deviation of high cloud responds directly to the standard deviation of high cloud. The bulge of data points in the middle of the plot which indicates a lack of correlation represents the middle latitude. The values of the high cloud standard deviation depict the variation in high cloud amount. However, the IR standard deviation is responding, not only to the variability of IR from the high cloud but to the variability of IR from the underlying surface as well. This response of standard deviation of IR is evident because the middle latitudes are characterized predominantly by seasonal high cloud amount of less than 25%.

5.2.2 Regional Analyses

Figures 5.5 through 5.8 represent the regression analyses for the mean and standard deviation fields of high cloud and IR with the effects of the midle latitudes are removed. The result is a more linear correlation between the two fields than depicted by the global analyses due to a strong signal between IR and high cloud in this region.

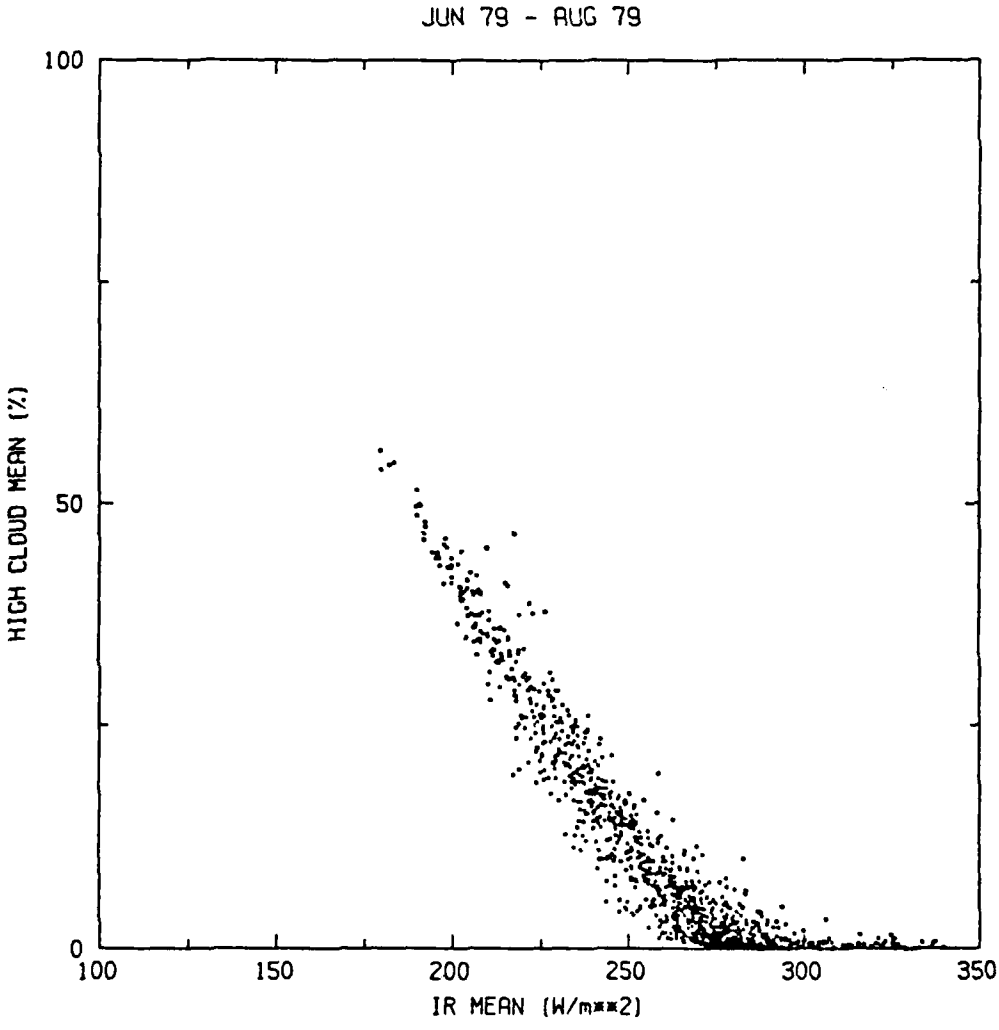

Figure 5.5 Regression analysis of IR mean vs. high cloud mean for NH Summer (31.5°N - 31.5°S).

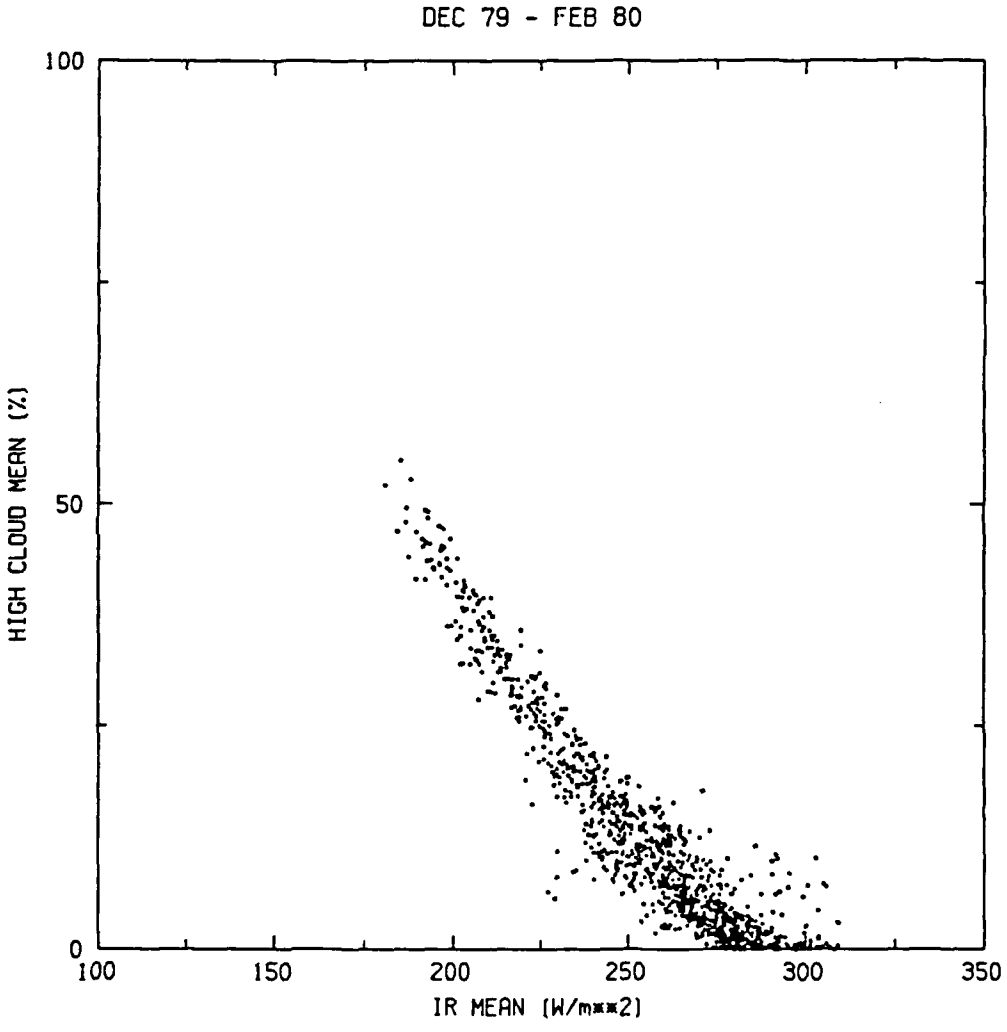

Figure 5.6 Regression analysis of IR mean vs. high cloud mean for NH Winter (31.5°N - 31.5°S).

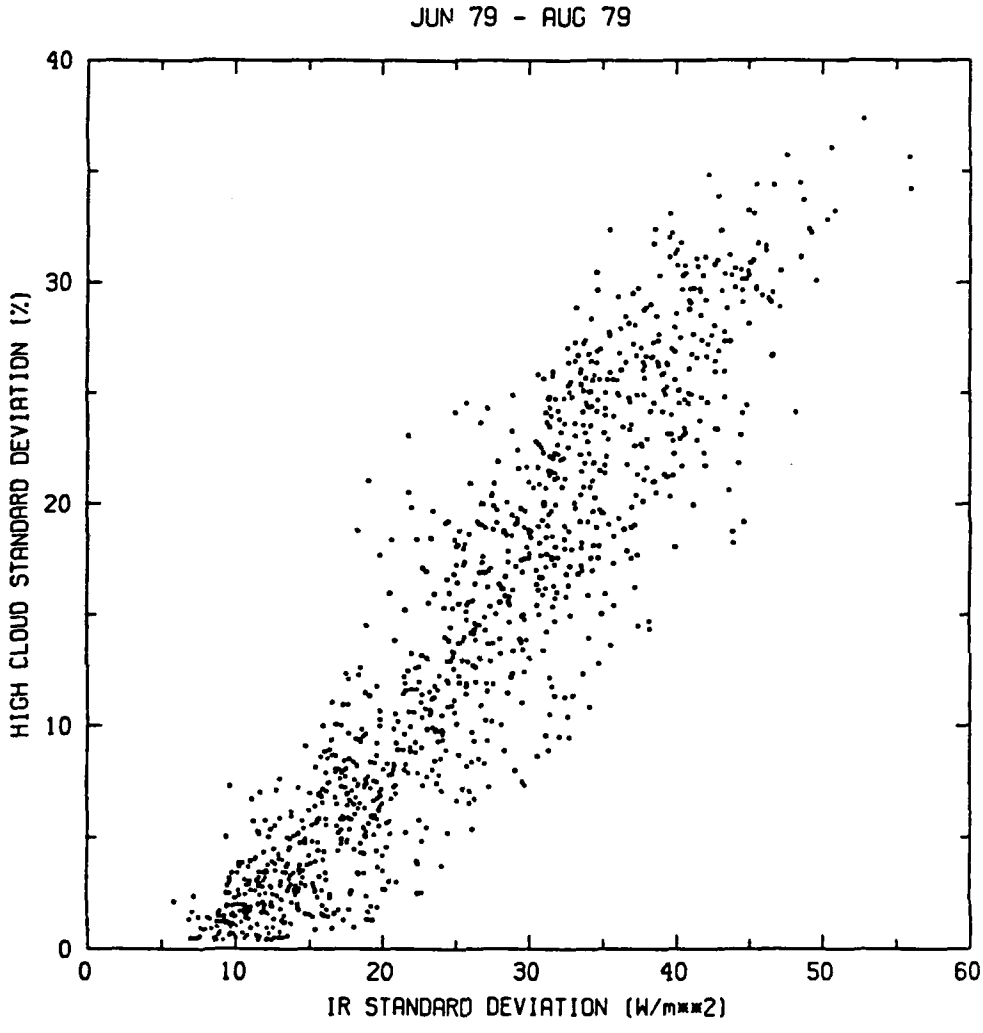

Figure 5.7 Regression analysis of IR standard deviation vs. high cloud standard deviation for NH Summer (31.5°N - 31.5°S).

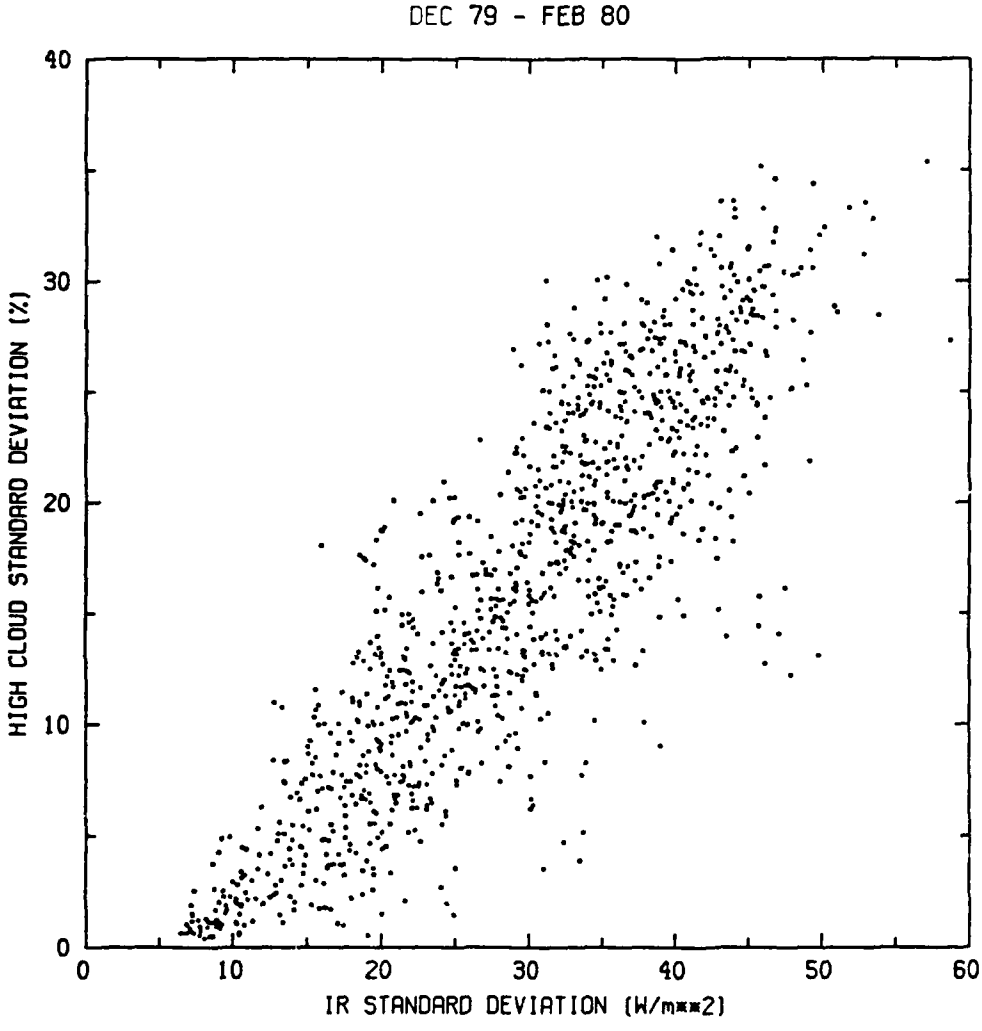

Figure 5.8 Regression analysis of IR standard deviation vs. high cloud standard deviation for NH Winter (31.5°N - 31.5°S).

The correlation between the mean fields of IR and high cloud for the summer and winter seasons are shown in Figures 5.5 and 5.6, respectively. A strong negative correlation is evident for both seasons. Data points representing large amounts of cloud and low IR values is associated with the cloudy ITCZ while low cloud amounts and large IR values represent the dry subtropical areas. Note that during the NH summer season, values of IR for zero cloud amount exceed those cloud-free IR values during the NH winter. The values during the summer represent the desert regions of northern Africa where substantial surface heating occurs resulting in large loss of IR to space. During the SH summer, since land surfaces are not as abundant in the SH, the IR lost to space is not as intense.

Figures 5.7 and 5.8 depict the regression analyses of the standard deviation fields for the IR and high cloud during the NH summer and winter respectively. These analyses indicate a positive correlation for both seasons. The NH summer analysis show a better correlation due to the strong signal of high cloud and IR emerging from the Asian monsoon and African desert areas.

5.2.3 Subregional Analyses

The regression analyses for high cloud and IR over ocean and land areas of the cloudy ITCZ are shown in Figures 5.9 and 5.10 respectively. Even though these regions are characterized by a large amount of cloud in the seasonal mean, it is indicated in these graphs that there is a day to day fluctuation of high cloud cover and IR during the period. Recall that the standard deviation of high cloud and IR over these regions is large. There appears to be little difference between the analyses over land and ocean. However, IR values range from about 120 W/m^2 to 302 W/m^2 over land while over the ocean, they range from about 103 W/m^2 to 285 W/m^2. This is an indication of the more intense heating of land surfaces compared to ocean surfaces and hence a stronger IR flux to space over the land.

Figures 5.11 and 5.12 show the correlation of high cloud and IR over ocean and land areas, respectively, for cloud-free regions within the low latitudes. Note that there is much less variation of cloud cover and IR compared to the cloudy ITCZ regions. This appears to be especially true over the ocean area.

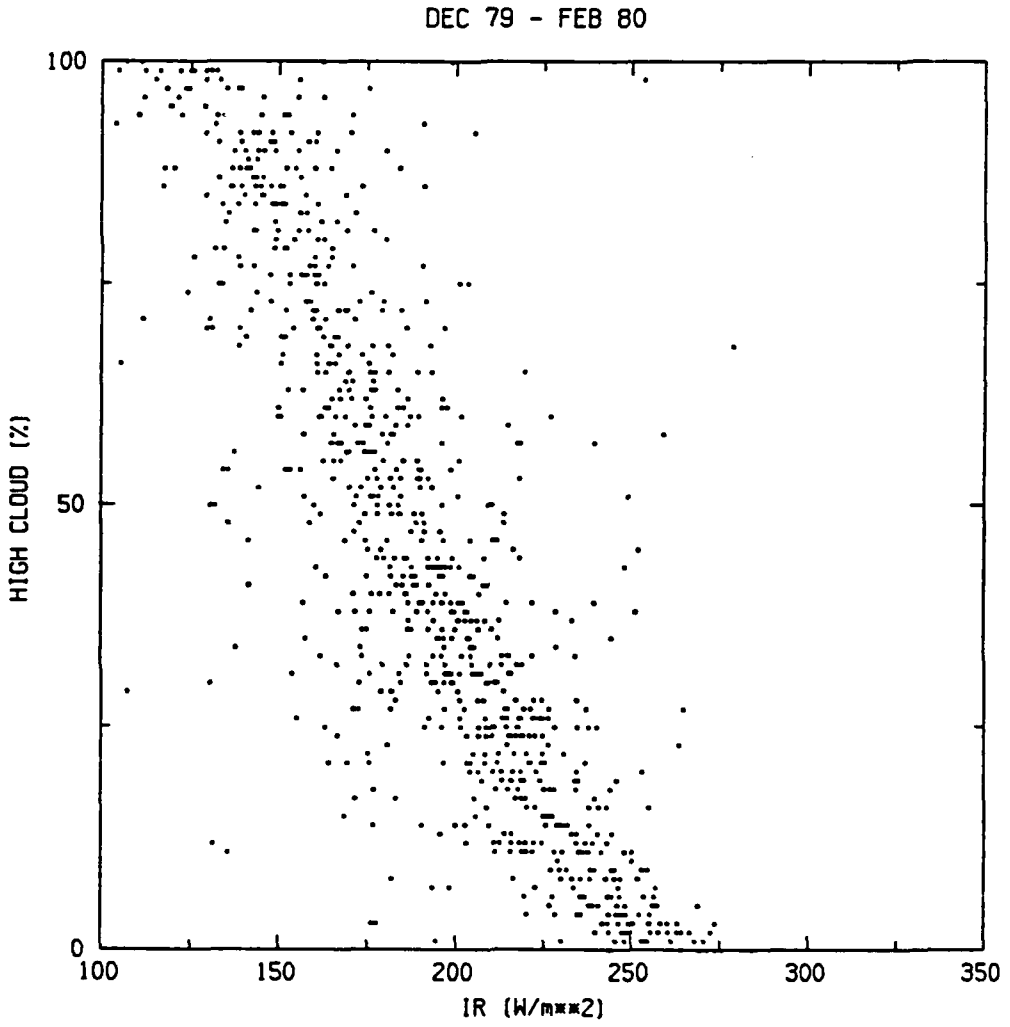

Figure 5.9 Regression analysis of daily IR vs. high cloud for NH Winter (Cloudy Ocean Area).

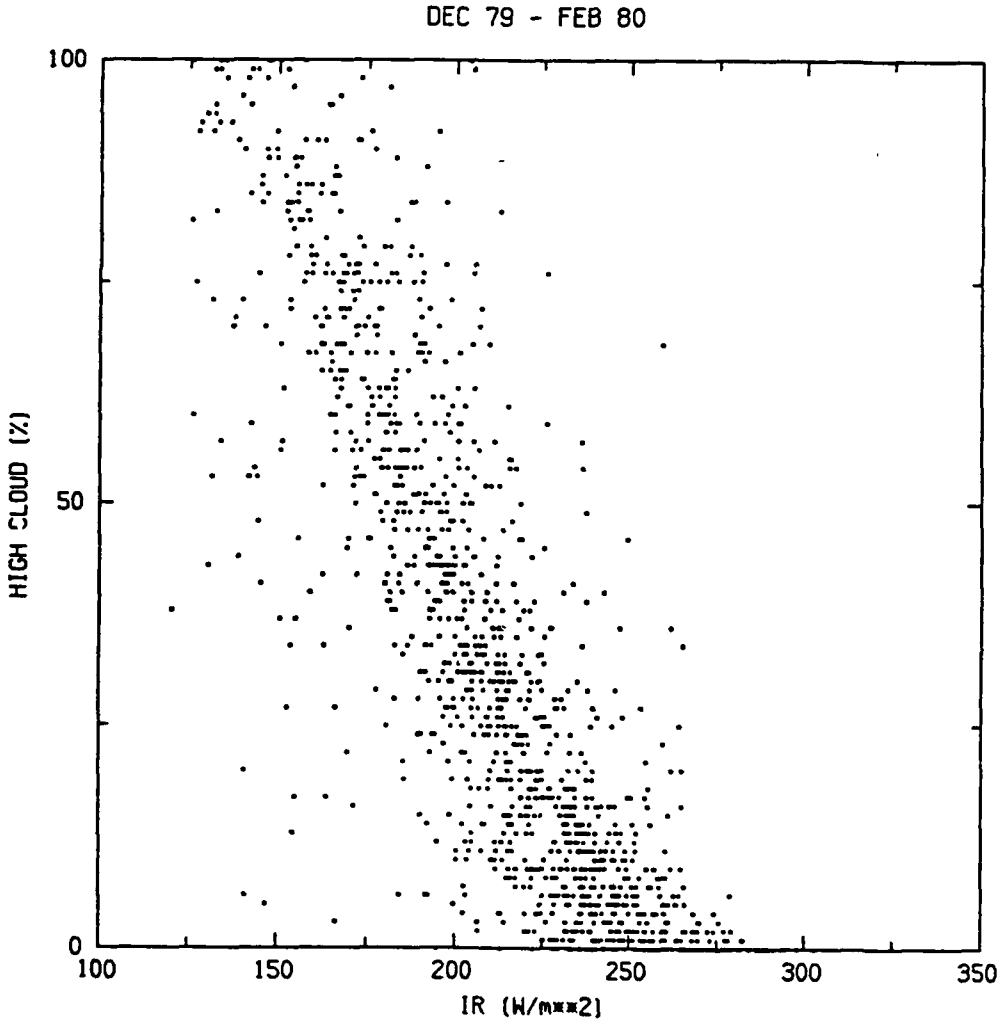

Figure 5.10 Regression analysis of daily IR vs. high cloud for NH Winter (Cloudy Land Area).

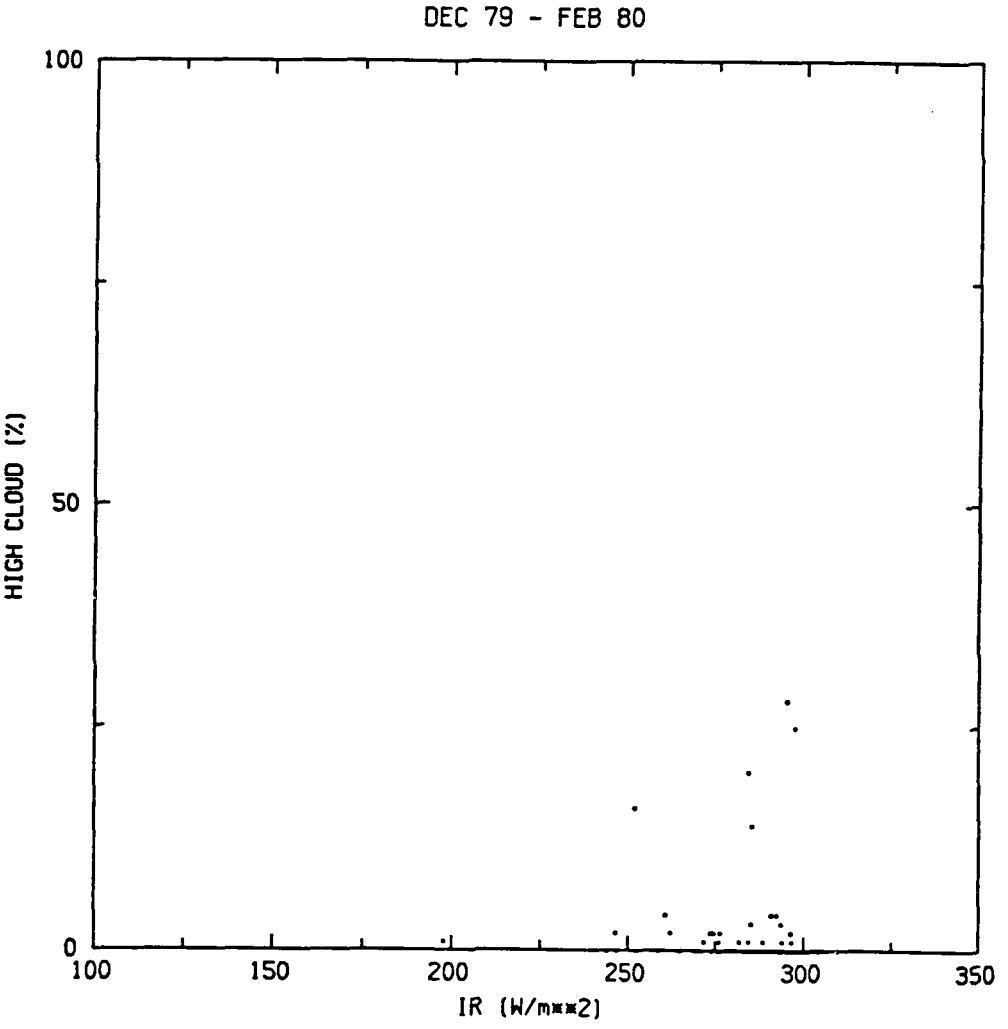

Figure 5.11 Regression analysis of daily IR vs. high cloud for NH Winter (Clear Ocean Area).

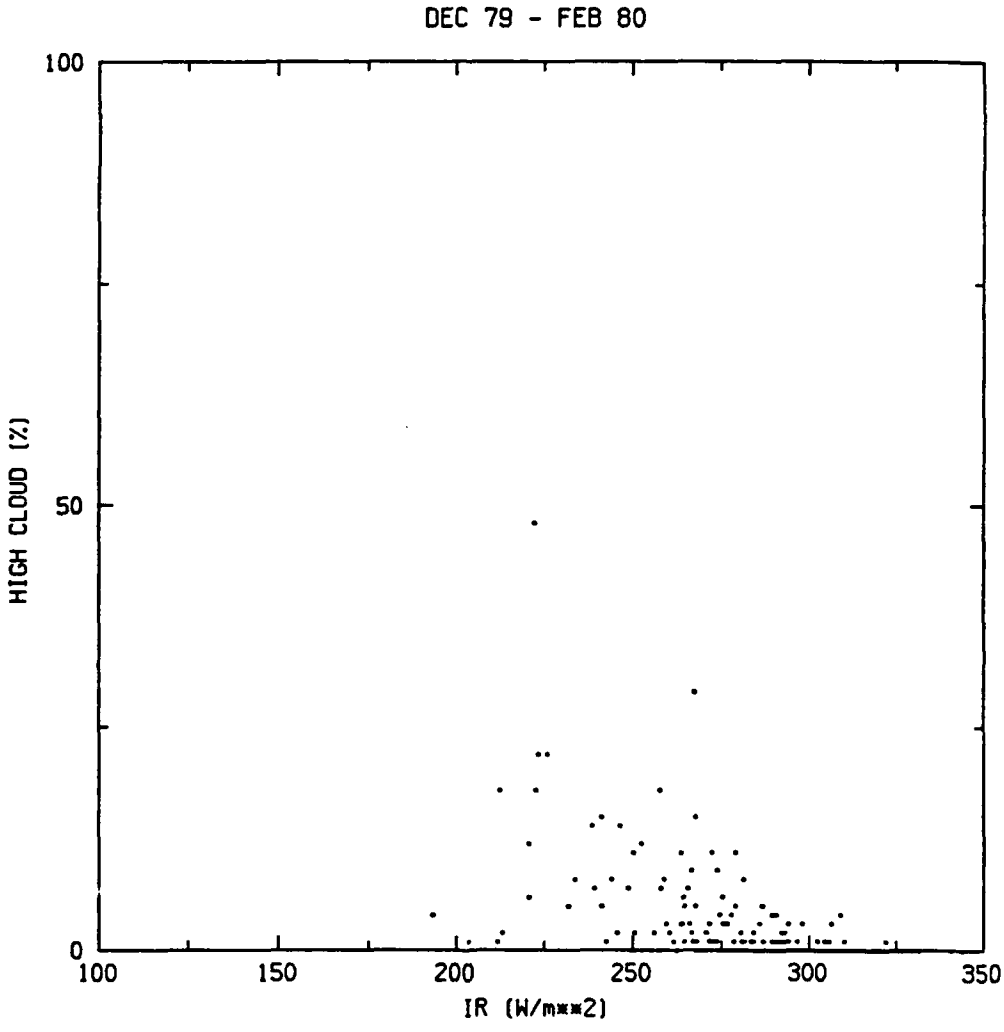

Figure 5.12 Regression analysis of daily IR vs. high cloud for NH Winter (Clear Land Area).

6.0 TOTAL CLOUD IR FLUX

Theoretically, the IR flux for a clear atmosphere over a specific area can be determined based on it surface temperature. In Chapter 5, I presented the measured variations of the IR emitted to space by the cloud-free plus cloudy atmosphere over chosen areas. When the effects of the cloud-free portion of the atmosphere are removed, the result is the actual IR emitted to space by the cloud alone. I will call this parameter the cloud IR flux. To study the correlation between total cloud cover and cloud IR, I have analyzed scatter diagrams between the two fields for six cases within the low latitudes where the signal between IR and cloud is the strongest. I used three land three ocean areas for clear and cloudy cases and for transition zones between clear and cloudy regions.

6.1 Procedure

To determine the contribution of cloud to IR measurements, it is first necessary to determine a cloud-free IR. This is obtained by selecting, the day of least amount of total cloud cover during a season for each grid point over the globe. Next, the IR value corresponding to the day of minimum cloud cover is chosen. This value is the maximum measured IR or cloud-free IR during a season. Finally the difference between the maximum IR and cloudy (measured) IR is calculated for each grid resulting in the IR contributed by the total cloud cover, i.e., the cloud IR or ΔIR.

The maximum IR chosen is not in actuality a cloud-free IR value for all locations. Over areas of the globe which are characterized by abundant cloudiness during a season, such as the ITCZ, the maximum IR is taken from the day which indicates least cloud cover. If a grid never exhibits a day of zero cloud cover, then the cloud-free IR is merely the maxmum IR obtained for that grid corresponding to the day of least amount of cloud cover.

6.2 Case Studies

Figure 6.1 depicts the correlation between total cloud and cloud IR for the cloudy monsoon region over the Indian Ocean, and Figure 6.2 shows the relationship for a cloudy region over South America. These regions are characterized by a seasonal mean of total cloud of 80% or greater and mean IR values of less than 275 W/m^2. Both plots are similar and depict the expected results in two regards. First, for low amounts of cloud, the cloud-free IR chosen is close to the cloudy IR value measured. The result is a small value of ΔIR. Second, in situations of large amount of cloud cover, the determined cloud-free IR values are larger than the actual measured IR resulting in a large value for ΔIR. However, data points representing low IR and large cloud amounts indicate that for a large amount of cloud cover, the difference between cloudy and cloud-free IR values is small. Recall that over the cloudy tropical regions there is a large amount of total cloud with a small variation, but there is also a large amount of high cloud with a large variation. When the high cloud amount is small, this allows for the satellite to view the mid and low level clouds. As discussed in Chapter 5, these lower altitude clouds contribute a large IR flux to space due to their high temperatures. Therefore, when high cloud amount is small and lower altitude cloud cover is still large, the difference between cloud-free IR and cloudy IR is small. There is no apparent difference between the cloudy land and cloudy ocean area.

Figure 6.3 shows the correlation of total cloud and ΔIR for seasonally "clear" regions over the Pacific Ocean. Figure 6.4 shows this correlation for cloud-free regions over the desert of northern Africa. Of course, these regions are not always clear of all cloud cover. They are characterized by a seasonal amount of total cloud of less than 20%. In both figures, it is evident that the correlation between the two fields results in a cluster of points depicting low cloud amounts in relation to small ΔIR values. Since these areas are characterized by low amount of cloud cover, the chosen maximum IR is very near the maximum possible value over the areas. This results in the small ΔIR values for most of the cases. The regression diagram over the ocean area depicts that there is also a small ΔIR value for times of increased cloud cover over the clear regions. This is a result of occasional intrusion of low level cloud into the area, and as expected, it has little or no effect on the

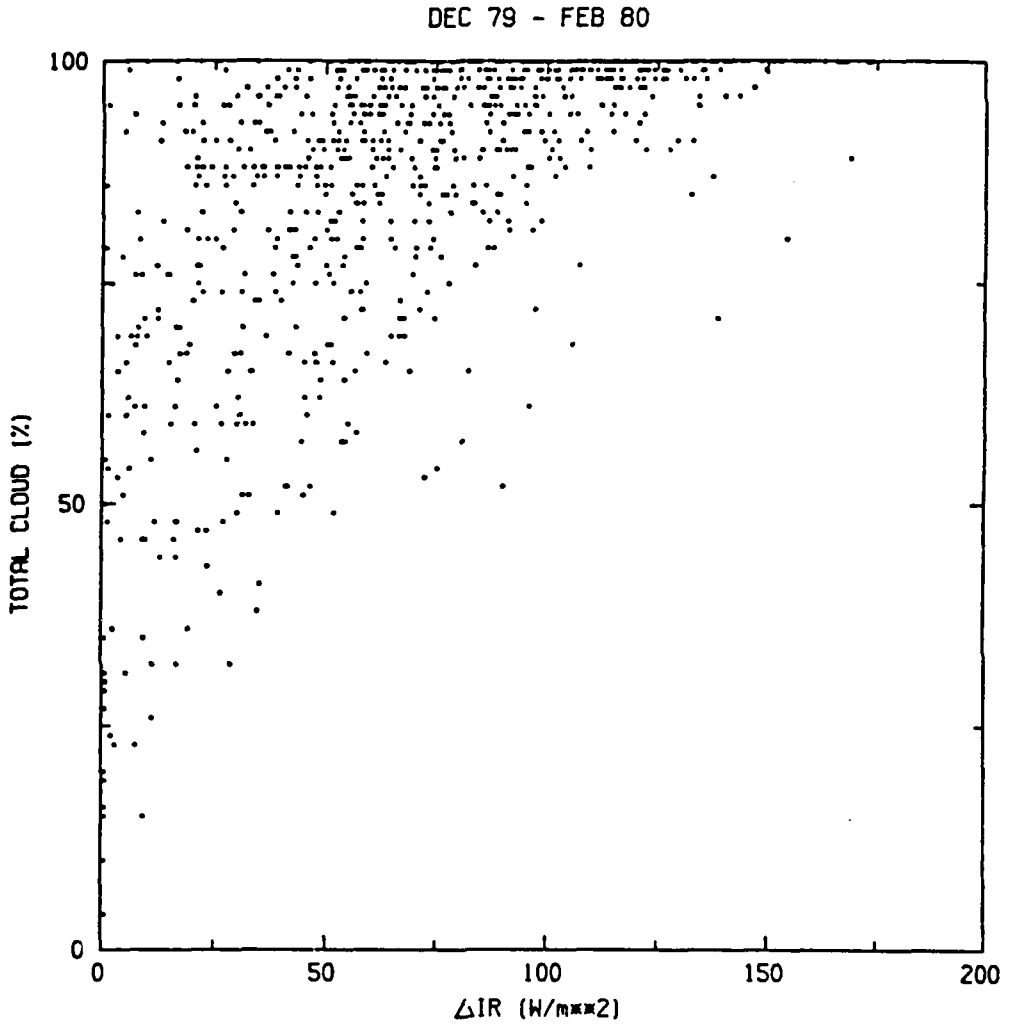

Figure 6.1 Regression analysis of daily total cloud vs. ΔIR for NH Winter (Cloudy Ocean Area).

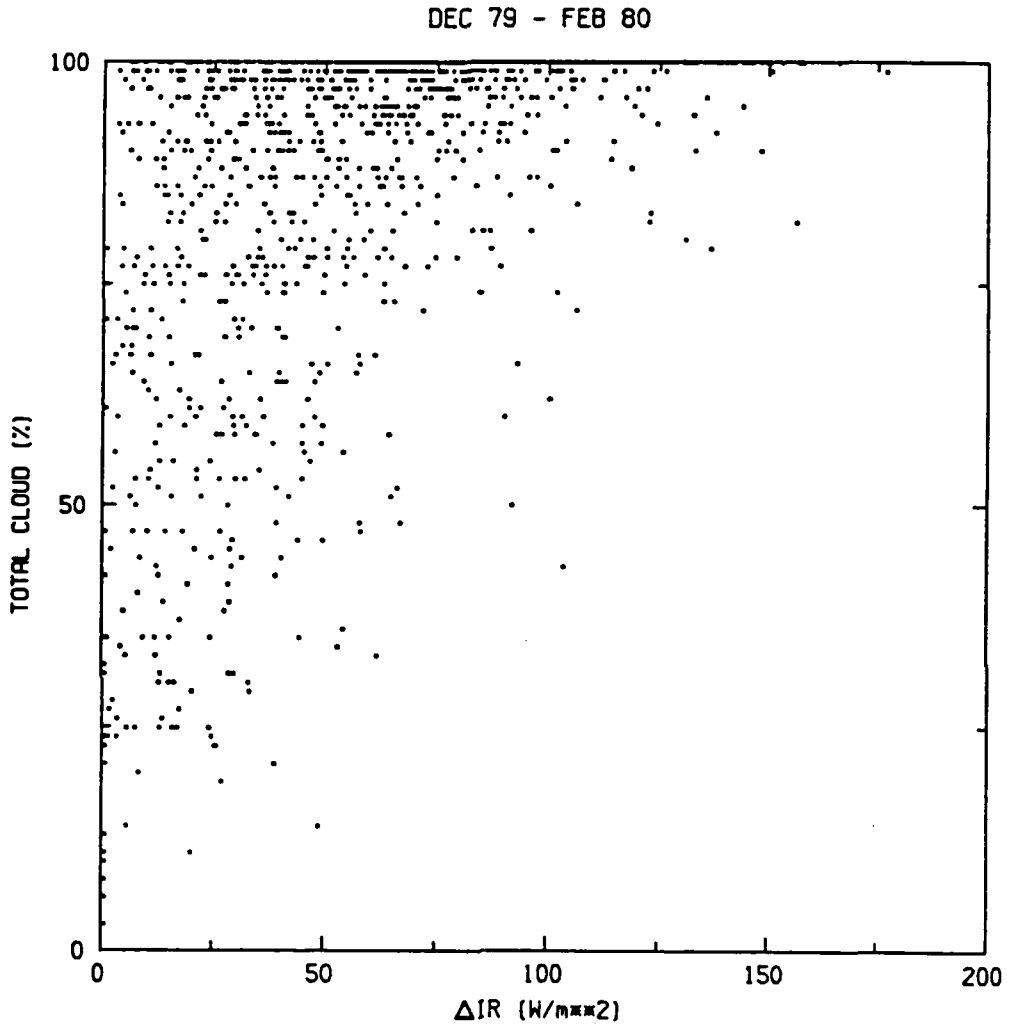

Figure 6.2 Regression analysis of daily total cloud vs. ΔIR for NH Winter (Cloudy Land Area).

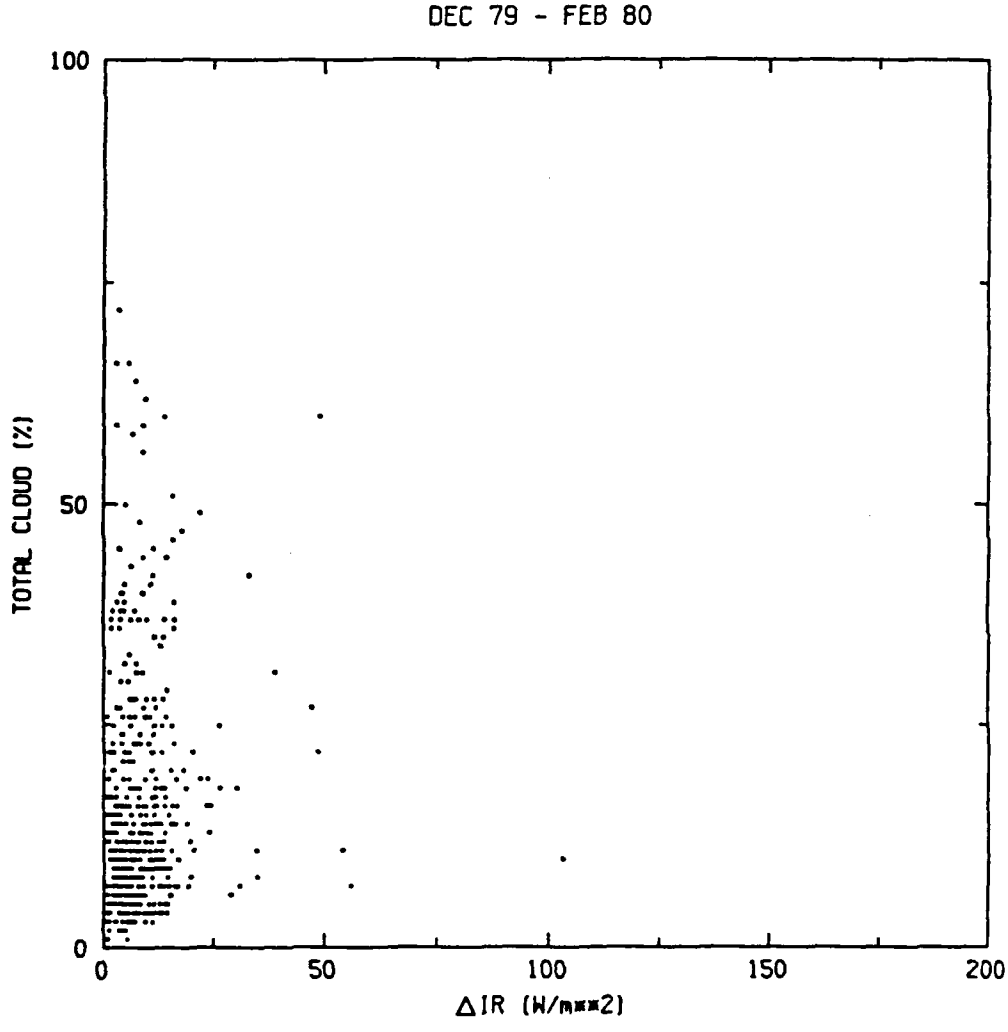

Figure 6.3 Regression analysis of daily total cloud vs. ΔIR for NH Winter (Clear Ocean Area).

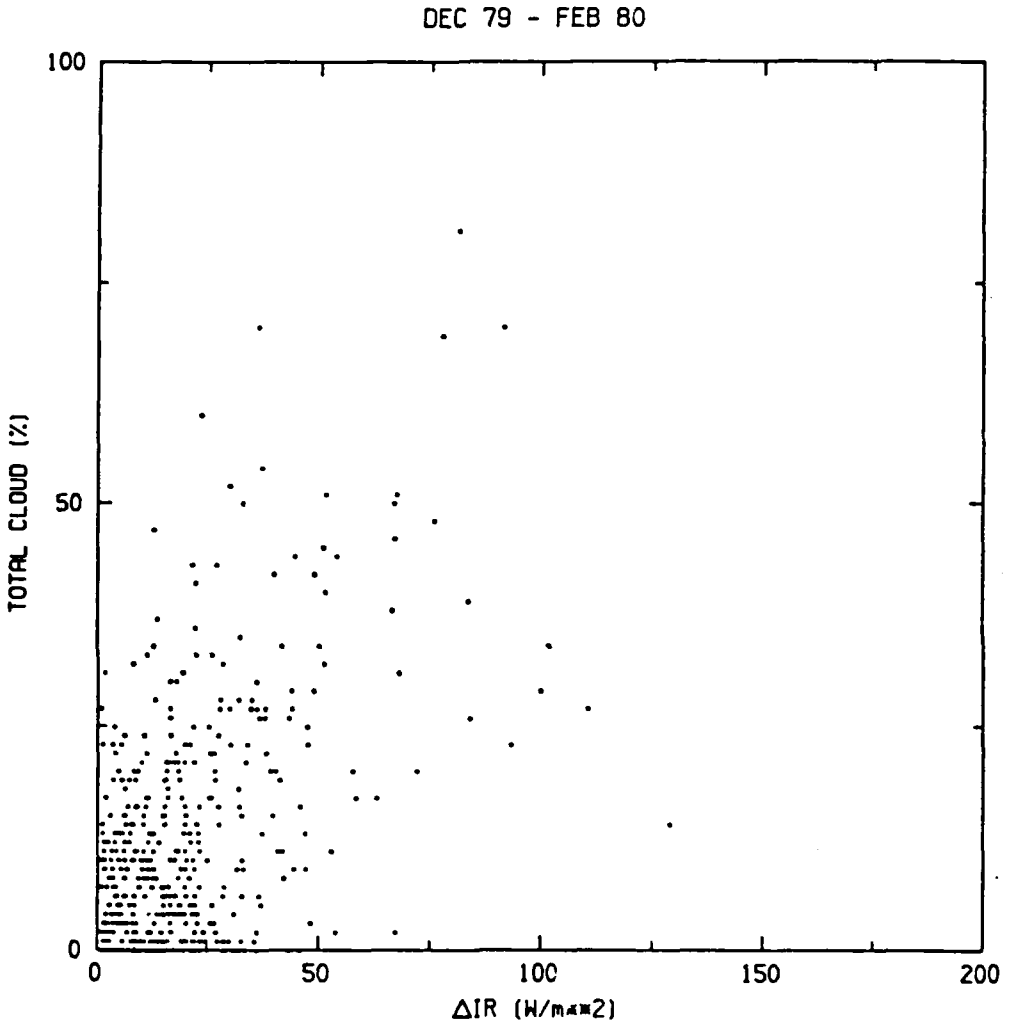

Figure 6.4 Regression analysis of daily total cloud vs. ΔIR for NH Winter (Clear Land Area).

IR. The scatter plot of the clear region over land indicates not only the presence of low cloud amount corresponding to a small ΔIR but also occasional occurences of high cloud with an anticipated decrease in cloudy IR and hence large IR values.

The third area of interest for this study is an area of transition between cloudy and clear regions. Recall that these areas of middle range amounts of total cloud cover is characterized by a large standard deviation of cloud and large standard deviation of IR. These areas are also characterized by a large amount and standard deviation of high cloud. Figure 6.5 is the scatter diagram betweeen total cloud and ΔIR over the Indian Ocean, and Figure 6.6 over central Africa. In both cases, the trend of a positive, linear correlation is evident. For small amounts of cloud cover, the calculated maximum IR closely correlates to the cloudy values, while for a large amount of cloud the differences between cloud-free and cloudy IR values is large. Hence, the effect of clouds on the IR at the top of the atmosphere is highly variable over these transition regions ranging from nearly zero for small amounts of cloud to greater than 175 W/m^2 for overcast conditions.

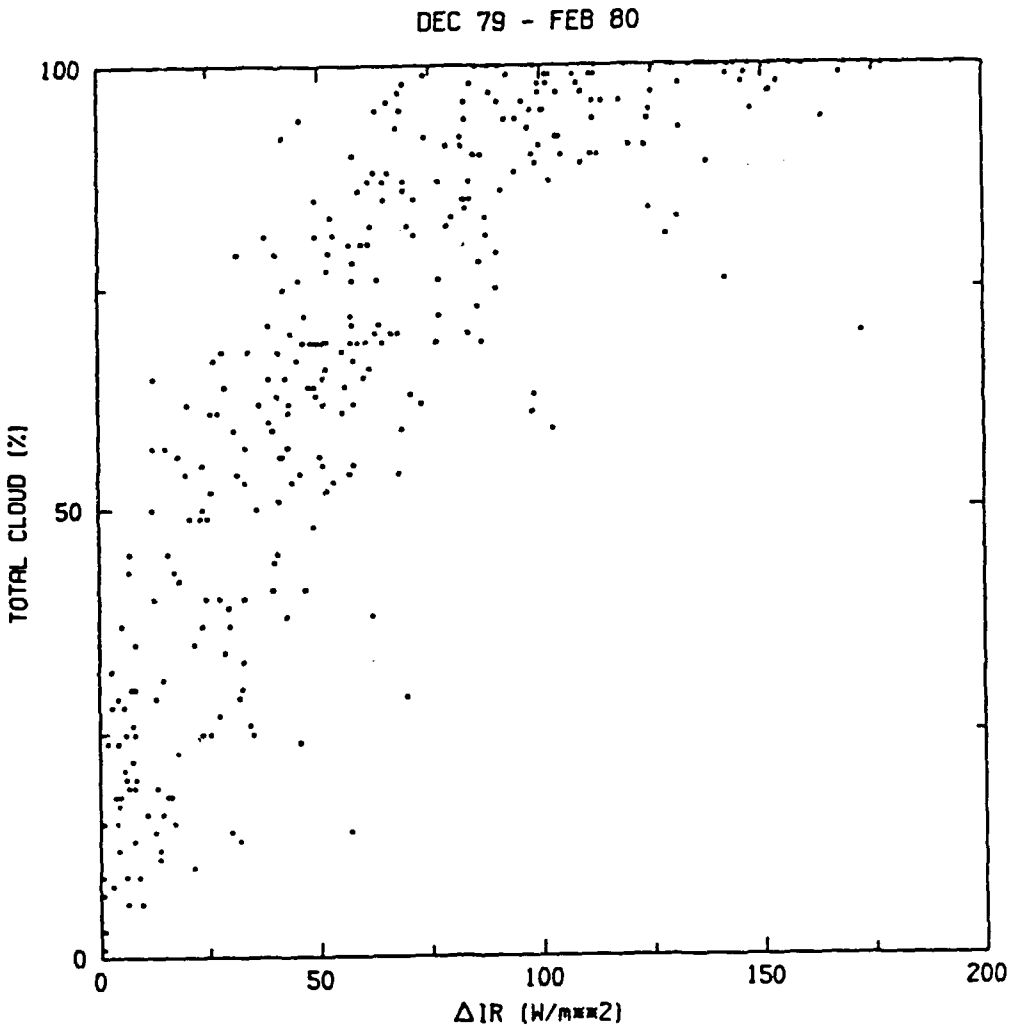

Figure 6.5 Regression analysis of daily total cloud vs. ΔIR for NH Winter (Transition Ocean Area).

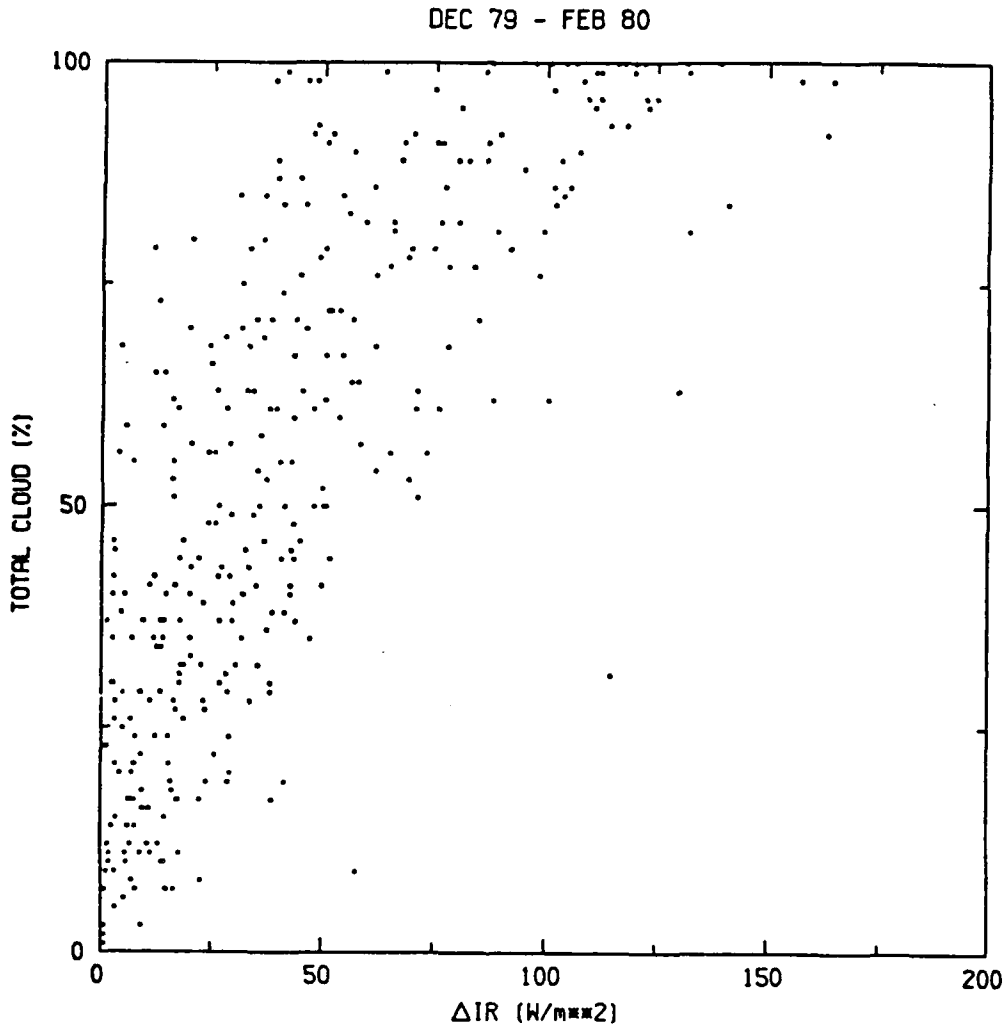

Figure 6.6 Regression analysis of daily total cloud vs. ΔIR for NH Winter (Transition Land Area).

7.0 CONCLUSION

Past studies of the relationship between cloud and radiation parameters have produced some uncertain results. Continued studies of cloud and radiation parameters are needed to provide a more complete understanding of the role clouds play in climate processes and possible climate changes and to aid development of climate models. Cloud and radiation data have been obtained simultaneously from separate instruments aboard the NIMBUS 7 satellite with the intent of improving earlier results. In my study, I have analyzed separately the fields of total cloud, high cloud, IR, and finally, have presented a correlation between the cloud and IR parameters. The following conclusions from this study were made.

7.1 Seasonal Mean Cloud

Examination of the seasonal mean field of total cloud defines the ITCZ by a band of maximum cloud which shifts from one hemisphere to the other following the interannual variability of the sun. Due to the intense convective activity of the ITCZ, moisture penetrativeness into high altitues and is depicted as a shield of high cloud over the ITCZ.

The subtropical regions are defined by a minimum of both total cloud and high cloud. These regions contain the subtropical anticyclones and desert areas, both which rely on massive subsidence to balance the atmosphereic energy. The result is a drying of the atmosphere.

The middle latitudes of the SH depict a zonal pattern of total and high cloud in winter and summer due to the presence of a large ocean mass. However, in the NH where there is a greater land to ocean ratio, the winter storm tracks emerge as an area of larger total cloud amount. There is a large percentage of both total and high cloud defining the Aleutian and Icelandic Lows.

7.2 Seasonal Standard Deviation of Cloud

The standard deviation fields indicate that for regions characterized by a large amount of total cloud or a small amount of total cloud, the variation in cloud is also small. That is, cloudy areas tend to remain cloudy and clear regions tend to remain clear for the duration of the season. Large standard deviations define the cloud transition zones between maximum and minimum centers of total cloud where the gradient of cloud amount of large.

The standard deviation field for high cloud shows that the ITCZ regions, where high cloud amount is large, are also defined by a large standard deviation of high cloud due to the large variability of convective activity. The subtropical regions of small amount of high cloud depict a small standard deviation. Middle latitudes show a slight increase of high cloud variation from summer to winter due to the variability of the advective storm systems.

7.3 Seasonal Mean of IR

The seasonal mean of IR reveals that, as in the cloud field, the location of the ITCZ emerges along the equator. It is defined by a band of minimum IR values due to the large amount of high cloud emitting low values of radiation corresponding to their low radiative temperatures. In the subtropics, where cloud cover is small, the IR values are large especially over the SH anti-cyclones and NH deserts in summer. These large values are a result of the large surface temperatures. In the middle latitudes the IR pattern reflects the north-south gradient of surface tempeure in the winter. It does not reflect the expected low IR areas associated with winter storm tracks as the amount of high cloud is only relatively large. Therefore, the IR emitted is a strong function of the surface temperature.

7.4 Seasonal Standard Deviation of IR

The standard deviation fields of IR show that the ITCZ area is defined by large values responding to the large variation of high cloud. The subtropical areas of large IR are characterized by small values of standard deviation as these areas are defined by low amount

of high cloud. The middle latitudes are not well defined by the IR standard deviation field, but relatively large values emerge along the winter storm track in both hemispheres.

7.5 Regression Analyses of IR vs. High Cloud

Examination of regression analyses between the mean fields of high cloud and IR indicate the expected negative correlation for a portion of the graph. These points represent the low latitudes where there is a strong signal between high cloud and IR. Low values of IR corresponding to a large amount of high cloud cover emerge from the ITCZ regions. The IR emitted to space from this cloud region is a function of the low temperature of the cloud tops. Large values of IR corresponding to a small amount of high cloud emerge from the dry subtropical regions where the large IR values are a result of the transfer of radiation directly from the surface with very little interference from cloud cover. An interesting second "branch" emerges in the diagram indicating low IR values associated with low amounts of high cloud. These points represent the middle latitudes where, even without a large amount of high cloud, the IR values are low due to radiation being emitted from the cooler land surfaces.

The standard deviation fields between IR and high cloud indicate a positive correlation beteen IR and high cloud for the low latitudes. Areas of large variation of IR, the ITCZ, are responding to the large variation in high cloud amount associated with the convective activity. The dry subtropical areas are characterized by a small variation of IR responding to a small standard deviation of high cloud. A "bulge" of data points, disrupting the linear trend, emerge from the middle latitudes where the standard deviation of high cloud responds to the variability of high cloud. But the IR standard deviation responds to the variability of IR emitted from the surface as well as from the high cloud.

7.6 Regression Analyses of Total Cloud IR vs. Total Cloud

To study the amount of IR emitted from the cloud cover itself (ΔIR), the difference between the maximum IR values, corresponding to days of minimum total cloud cover, and measured IR values was computed. Regression analyses between IR and total cloud

for cloudy regions in low latitudes indicate the expected positive correlation for low ΔIR corresponding to low cloud amount and vice versa. Data points corresponding to low IR and large amounts of cloud also emerge on occasions when high cloud amount is small (small ΔIR) but the lower altitude cloud amount is still large.

Correlation between total cloud and ΔIR in clear regions depict a cluster of points corresponding to small cloud amount and small ΔIR. This arises due to the small variations in cloud cover and hence a small variation of IR over the region. That is, the chosen maximum IR value is observed most of the time.

Finally, the correlation between ΔIR and total cloud indicates a nearly linear positive correlation for regions of transition between maximum and minimum cloud cover. These areas are characterized by a large variation in cloud cover and IR. The characteristic large variation in cloud cover and IR allows for the maximum IR chosen to be well representative of a maximum IR value.

7.7 Summary

This research has been an observational study of the cloud and radiation data originating from different instruments aboard the NIMBUS 7 satellite. There have been extensive, yet separate, studies performed by different groups of scientists with each of these data sets. I have merged these two sets of data to derive a new data set of various measurements for cloud and longwave radiation in contribution to the climatology of cloud–radiation processes.

Use of quantitative and qualitative validation methods (Chapter 2) proved the NIMBUS 7 cloud data to be an accpetable, good set of data. My global analyses of cloud cover (Chapter 3) proved this data to be meteorologically sound with respect to climatological positions synoptic features. But how well does this cloud data compare to past cloud climatologies? It must first be considered that differences will occur due to the fact that the data set used covers only one year of data while climatologies are prepared using many years of information. A general comparison to the climatologies presented by Clapp (1964), Sadler (1969), and Becker (1979) provided good results with the following similarities observed:

a. areas of very clear skies over continental desert regions associated with the subsidence branch of the Hadley Cell;

b. a broad area of maximum cloudiness over India and Southeast Asia during July with a southward shift and decreased aerial coverage of the convection for January;

c. identification of the Aleutian and Icelandic vortices by maximum cloud amount with seasonal variation in size and latitudinal location;

d. a zonal distribution of cloud in the SH middle latitudes with small seasonal change; and

e. uncertainty of cloud estimates in the polar regions of both hemispheres due to lack of data or snow/ice coverage.

The most important result emerging from this study has been the differences between the low and middle latitudes when relating IR and cloud parameters. In the low latitudes where incoming solar radiation is most intense, well developed maximum and minimum centers of high cloud develop. The outgoing IR responds to the large difference in the radiative temperatures of the two areas resulting in a clear linear correlation between IR and high cloud for these latitudes. However, in the middle latitudes incoming solar radiation decreases with increased latitude, and maximum and minimum centers of high cloud become less defined. The outgoing IR tends to be more responsive to the north–south temperature gradient. The result is a more complex relationship between IR and high cloud with quantitative studies producing nonlinear and/or multiple correlations between the fields.

7.8 Suggestions for Future Research

The cloud and radiation data sets from the NIMBUS 7 satellite provide the opportunity for further interesting research outside the scope of this thesis. The cloud data can be used to present an in-depth cloud climatology with a comparison to others presented in the past, especially to those derived with satellite data.

A study of the tropical convective precipitation pattern as it related to cloud amount should be studied. Use of a ratio of high cloud to total cloud amount can provide infor-

mation in determining the onset of convective activity. The tropical convective areas also provide the opportunity to compare the relationship between the energy associated with precipitation and radiation, i.e., the latent heat release associated with the precipitation and IR emitted to space.

The middle latitudes, although somewhat complex, can provide an interesting study of the variability of IR to that of high cloud. Also, a comparison between the NH and SH can be performed providing information and perhaps a better understanding of the energy balance within this latitude region and the differences between processes in each hemisphere.

If in tropical regions it is assumed that the net IR at the surface is constant in time, use of the IR and high cloud data can provide information on the tropospheric cooling. Also, daily and seasonal variability of this cooling and the contribution of the cooling variance due to clouds can be studied.

REFERENCES

Adem, J., 1967: On the relations between outgoing long-wave radiation, albedo, and cloudiness. *Mon. Wea. Rev.*, **95**, 257–260.

Ahrens, C. D., 1985: Meteorology Today. West Publishing Company, 524 p.

Ardanuy, P. E., H. L. Kyle, 1986: El Nino and outgoing longwave radiation: Observations from NIMBUS 7 ERB. *J. Atmos. Sci.*, **114**, 415–433.

Arking, A., 1964: Latitudinal distribution of cloud cover from TIROS III photographs. *Science*, **143**, 569–572.

Becker, R. J., 1979: The global distribution of radiative heating and its retion to the large scale features of the general circulation. Ph.D. dissertation, University of Maryland, 201 p.

Cahalan, R. F., D. A. Short, and G. R. North, 1982: Cloud fluctuation statistics. *Mon. Wea. Rev.*, **110**, 26–43.

Campbell, G. G., and T. H. Vonder Haar, 1980: Climatology of radiation budget measurements from satellites. Atmospheric Science Paper No. 323, Colorado State University, Fort Collins, Colorado.

Cess, R. D., B. P. Briegleb, and M. S. Lian, 1982: Low latitude cloudiness and climate feedback: Comparitive estimates from satellite data. *J. Atmos. Sci.*, **39**, 53–59.

Cess, R. D., 1976: Climate change: An appraisal of atmospheric feedback mechanisms employing zonal climotology. *J. Atmos. Sci.*, **33**, 1831–1843.

Chang, C. P., 1970: Westward propagating cloud patterns in the tropical Pacific as seen from time-composite satellite photographs. *J. Atmos. Sci.*, **27**, 131–138.

Clapp, P. F., 1964: Global cloud cover for seasons using TIROS nephanalysis. *Mon. Wea. Rev.*, **92**, 495–507.

Coakley, J. A., Jr., and F. P. Bretherton, 1982: Cloud cover from high resolution scanner data: Detecting and allowing for partially filled fields of view. *J. Geophys. Res.*, **87**, 4917–4932.

Cox, S. D., 1971: Cirrus cloud and the climate. *J. Atmos. Sci.*, **28**, 1513–1515.

Dopplick, T. G., 1972: Radiative heating of the global atmosphere. *J. Atmos. Sci.*, **29**, 1278–1294.

Ellis, J. S., 1978: Cloudiness, the planetary radiation budget, and climate. Ph.D. dissertation, Department of Atmospheric Science, Colorado State University, 129 p.

Gordon, C. T., R. D. Hovanec, and W. F. Stern, 1984: Analyses of monthly mean cloudiness and their influence upon model-diagnosed radiative fluxes. *J. Geophys Res.*, **89**, 4713–4738.

Hartmann, D. L., and D. A. Short, 1980: On the use of earth radiation budget statistics for studies of clouds and climate. *J. Atmos. Sci.*, **37**, 1233–1250.

Hobbs, P. V., 1981: Clouds: Their Formation, Optical Properties, and Effects. Academic Press, 497 p.

House, F. B., 1985: Observing the earth radiation budget from satellites: Past, present, and future. *Adv. Space Res.*, **5**, 89–98.

Hughes, N. A., 1984: Global cloud climatologies: A historical review. *J. Climate Appl. Meteor.*, **23**, 724–751.

Hughes, N. A., and A. Henderson-Sellers, 1983: The effect of spatial and temporal averaging on sampling strategies for cloud amount data. *Bull. Amer. Meteor. Soc.*, **64**, 250–257.

Hughes, N. A., and A. Henderson-Sellers, 1985: Global 3-D nephanalysis of total cloud amount: Climatology for 1979. *Bull. Amer. Meteor. Soc.*, **24**, 669–686.

Hwang, P. H., ed., 1982: NIMBUS 7 Temperature Humidity Infrared Radiometer (THIR) Data User's Guide, NASA/GSFC, Greenbelt, MD, 52 p.

Jacobowitz, H., R. J. Tighe, and the NIMBUS 7 ERB Experiment Team, 1984: The Earth Radiation Budget derived from the NIMBUS 7 experiment. *J. Geophys. Res.*, **89**, 4997-5010.

Lau, K. M., and P. H. Chan, 1983: Short term climate variability and atmospheric teleconnections from satellite observed outgoing infrared longwave radiation. Part I: Simultaneous relationships. *J. Atmos. Sci.*, **40**, 2735-2750.

Lau, K. M., and P. H. Chan, 1983: Short term climate variability and atmospheric teleconnections from satellite observed outgoing infrared longwave radiation. Part II: Lagged correlations. *J. Atmos. Sci.*, **40**, 2751-2767.

Ohring, G., 1978: Some experiments with a zonally averaged climate model. *J. Atmos. Sci.*, **35**, 186–205.

Ohring, G., P. F. Clapp, T. R. Heddinghaus, and A. F. Krueger, 1981: The quasi-global distribution of the sensitivity of the earth atmosphere radiation budget to clouds. *J. Atmos. Sci.*, **38**, 2539–2541.

Ohring, G., and P. Clapp, 1980: The effect of changes in cloud amount on the net radiation at the top of the atmosphere. *J. Atmos. Sci.*, **37**, 447–454.

Randel, D. L., 1983: Space-time variations in the Earth Radiation Budget, Atmospheric Science Paper No. 374, Colorado State University, Fort Collins, Colorado.

Rossow, W. B., ed., 1981: Clouds in climate: Modelling and satellite observation studies. Report of workshop held at NASA Goddard Institute for Space Studies, New York, 222 p.

Rossow, W. B., F. Mosher, E. Kinsella, A. Arking, M. Desbois, E. Harrison, P. Minnis, E. Ruprecht, G. Seze, C. Simmer, and E. Smith, 1985: ISSCP cloud algorithm intercomparison. *J. Appl. Meteor.*, **24**, 877–903.

Ruprecht, E., 1985: Statistical approaches to cloud classification. *Adv. Space Res.*, **5**, 151–164.

Sadler, J. C., 1969: Average Cloudiness in the Tropics from Satellite Observations, International Indian Ocean Expedition. Meteor. Monogr. No. 2, East-West Center Press, Honolulu, 22 p.

Sellers, W. D., 1965: Physical Climatology. The University of Chicago Press, 272 p.

Schneider, S. H., 1972: Cloudiness as a global climatic feedback mechanism: The effects on the radiation balance and surface temperature of variations in cloudiness. *J. Atmos. Sci.*, **29**, 1413–1422.

Smith, L. D., and T. H. Vonder Haar, 1987: Temporal variability of the Earth Radiation Budget from NIMBUS 7 NFOV data: Comparison between NOAA and NIMBUS 7 polar orbiting satellites. Preprints, Third Conference on Satellite Meteorology and Oceanography, Anaheim, CA, American Meteorological Society, 142–147.

Stowe, L. L., 1984: Evaluation of NIMBUS 7 THIR/CLE and Air Force three-dimensional nephanalysis estimates of cloud amount. *J. Geophys. Res.*, **89**, 5370–5380.

Stowe, L. L., P. P. Pellegrino, P. H. Hwang, P. K. Bhartia, T. F. Eck, C. S. Long, C. G. Wellemeyer, H. Y. M. Yeh, 1986: Spatial and temporal characteristics of global cloud cover as observed from the NIMBUS 7 satellite. Extended Abstracts, Sixth Conference on Atmospheric Radiation, Williamsburg, VA, American Meteorological Society, 99–102.

Stowe, L. L., P. P. Pellegrino, P. H. Hwang, P. K. Bhartia, T. F. Eck, C. G. Wellemeyer, S. M. Read, and C. S. Long, 1986: Use of NIMBUS 7 satellite data for validation of GCM generated cloud cover. Workshop on Cloud Cover Parameterization in Numerical Models, 295–309.

Stowe, L. L., P. P. Pellegrino, C. G. Wellemeyer, T. F. Eck, H. Y. M. Yeh, and the NIMBUS 7 Cloud Data Processing Team, 1986: NIMBUS 7 global cloud climatology. Part I: Algorithms and Validation.

Trewartha, G. T., and L. H. Horn, 1980: An Introduction to Climate. McGraw-Hill, Inc., 416 p.

Welch, T. M., S. K. Cox, and J. M. Davis, 1980: Solar Radiation and Clouds. American Meteorological Society, Boston, Massachusetts.

Wetherald, R. T., and S. Manabe, 1980: Cloud cover and climate sensitivity. *J. Atmos. Sci.*, **37**, 1485–1510.

Yeh, H. Y. M., P. H. Hwang, T. F. Eck, C. G. Wellemeyer, P. K. Bhartia, L. L. Stowe, and C. S. Long, 1986: Intercomparison between NIMBUS 7 cirrus cloud data and ERB measurements. Extended Abstracts, Sixth Conference on Atmospheric Radiation, Williamsburg, VA, American Meteorological Society, 276–279.

APPENDIX A

TIME SERIES OF HIGH CLOUD:

The variation in time of the zonally averaged high cloud (Figure A.1) strongly reflects that of the total cloud cover. The most prominent feature of this time series is the tight gradient over the high latitude regions of the NH from Sep through May associated with a maximum cloud amount. As explained in the previous section, this is a result of the very cold surface temperatures being interpreted as cloud cover. In this time series, it is seen that the majority of the cloud is interpreted to be high cloud due to such low temperatures.

The high cloud associated with the ITCZ is evident positioned in the SH Dec through Mar and in the NH the remainder of the year. More than 20% of the ITCZ is shown to be covered with high cloud (60% to 70% is total cloud). This is a result of the cumulonimbus rising into high altitudes and spreading into extensive cirrus shields.

The NH middle latitues are characterized by a relative maximum of high cloud during most of the year. The slight decrease observed Feb through May north of 50°N is the result of the anticyclone which forms over the land masses at these latitudes. In the SH middle latitudes, there is little variation in time of high cloud amount.

As expected, high cloud over the subtropics is minimal. This minimum is most clearly defined during the winter seasons when the ITCZ moves into the summer hemisphere. Since the subtropical anticyclones are more intense during the summer, it may be expected that this cloud-free region be more pronounced during this season. However, the monsoon is also more intense with its high cloud cover spreading into the subtropical latitudes during the winter. As a result of zonal averaging, the boundries of the subtropical regions become less pronounced during the summer.

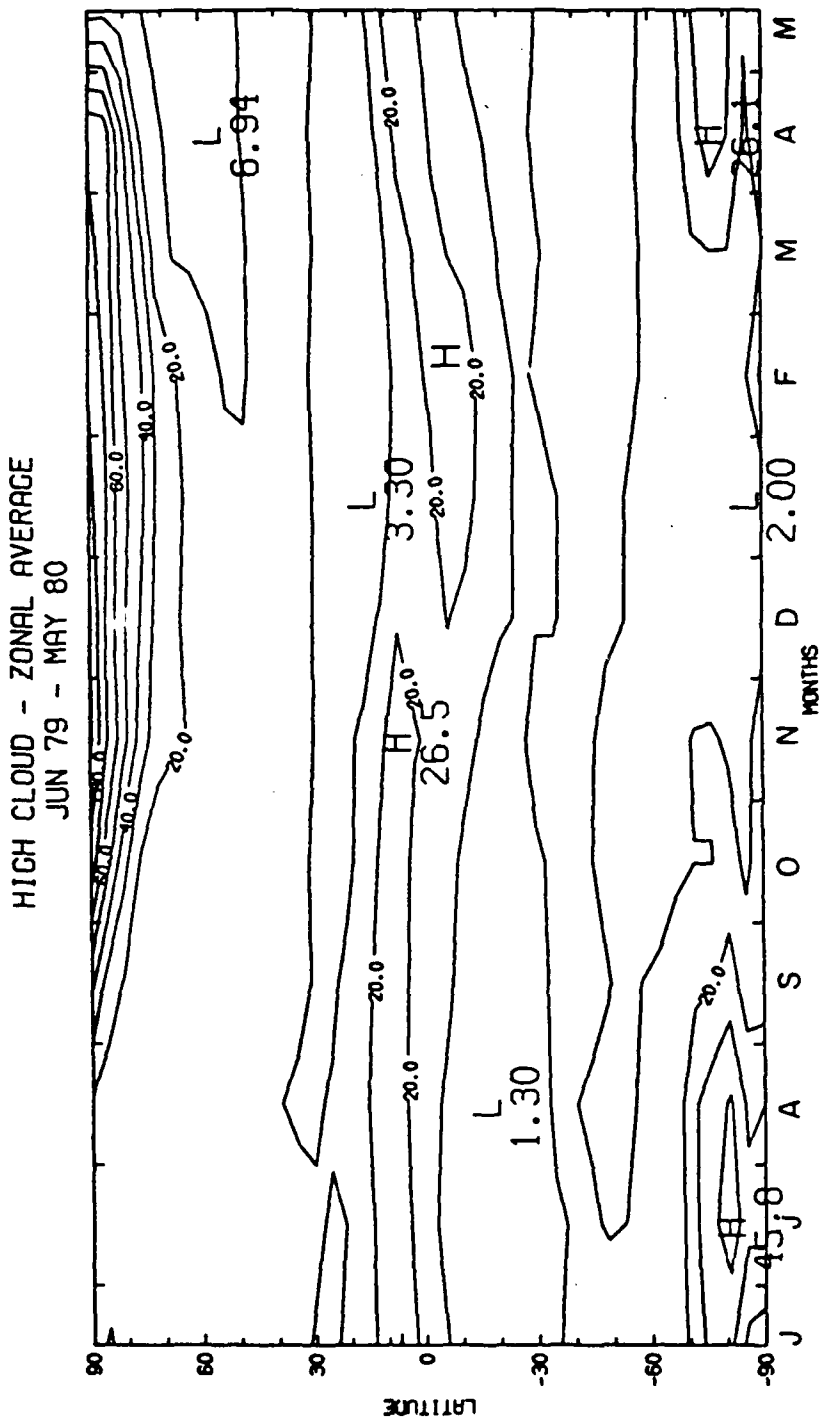

Figure A.1 Time-latitude cross section of zonally averaged high cloud amount.

APPENDIX B

TIME SERIES OF MIDDLE CLOUD:

The time series for the middle (mid) cloud (Figure B.1) is somewhat identical to that for the high cloud with a maximum amount of cloud identifying the ITCZ (>39%) and middle latitudes and a minimum in the subtropics. However, there is one very apparent difference. The time period during which the high latitude regions of the NH was covered with high cloud is shown to be a minimum for mid cloud. As discussed in sections 3.1.1 and 3.1.2, the satellite is detecting high cloud in this region due to the low temperatures, and no temperature high enough to be classified as mid or low cloud is detected in the polar atmosphere.

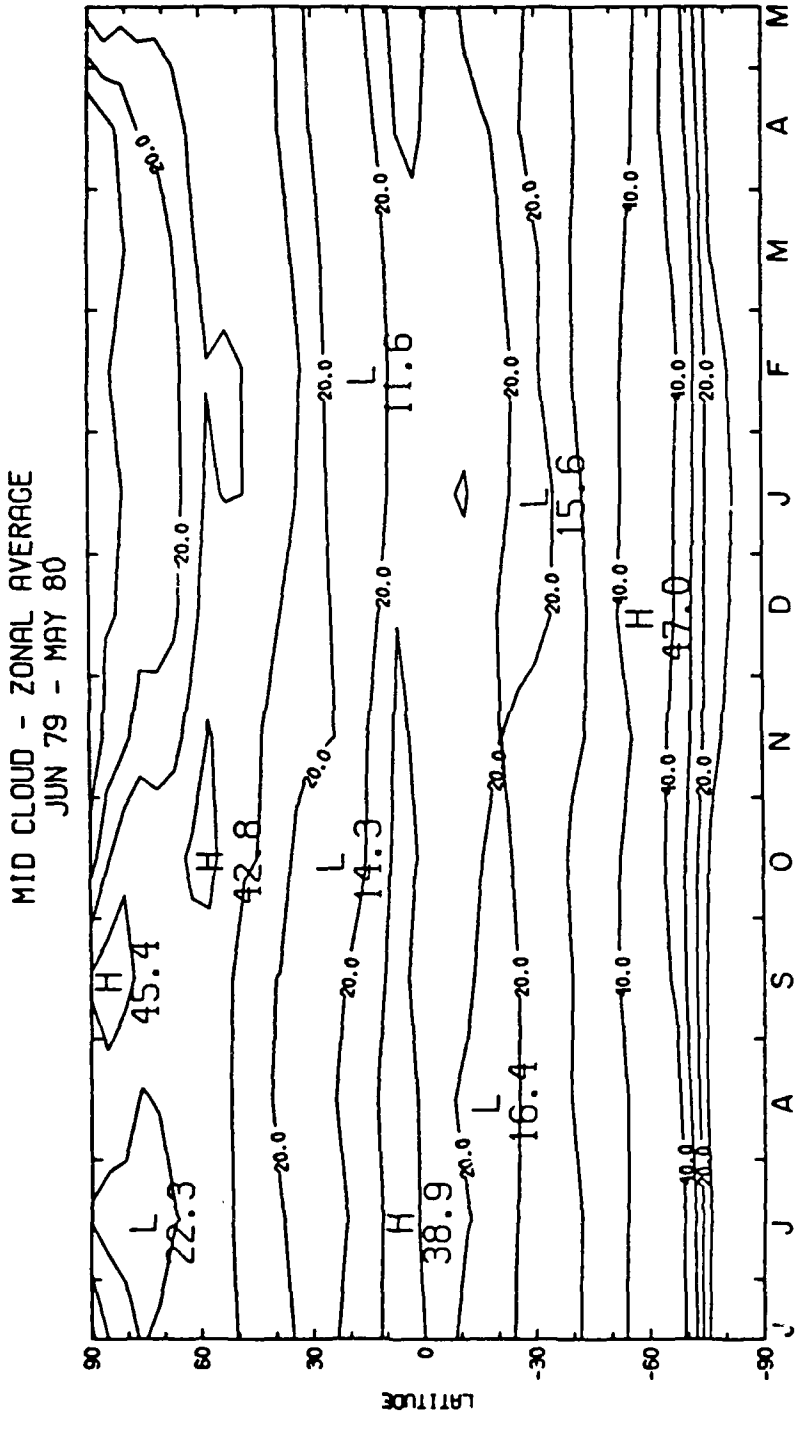

Figure B.1 Time-latitude cross section of zonally averaged middle cloud amount.

APPENDIX C

TIME SERIES OF LOW CLOUD:

The low cloud time series (Figure C.1) depicts a minimum of cloud cover over the ITCZ, the region characterized by a large amount of high and mid cloud. Even though a significant amount of low cloud does prevail within the ITCZ, the intense convective buildup of multi-layered clouds acts to obstruct the satellite's view of the low level cloud. The smallest cloud amounts exist in the region of the NH ITCZ (<10%) during the period Jun through Dec. However, this characteristic is not evident in the SH summer over the ITCZ region. This is due to increased higher altitude clouds during the NH summer monsoon when convection within the ITCZ is at its maximum over the southeast Asia.

Due to the extreme minimum over the NH ITCZ, there is the impression of increased low cloud amount in the subtropical regions. Middle latitudes of the SH depict a low cloud maximum (>20%) throughout the duration of the time series, while the NH middle latitudes are depicted by low cloud of less than 20%.

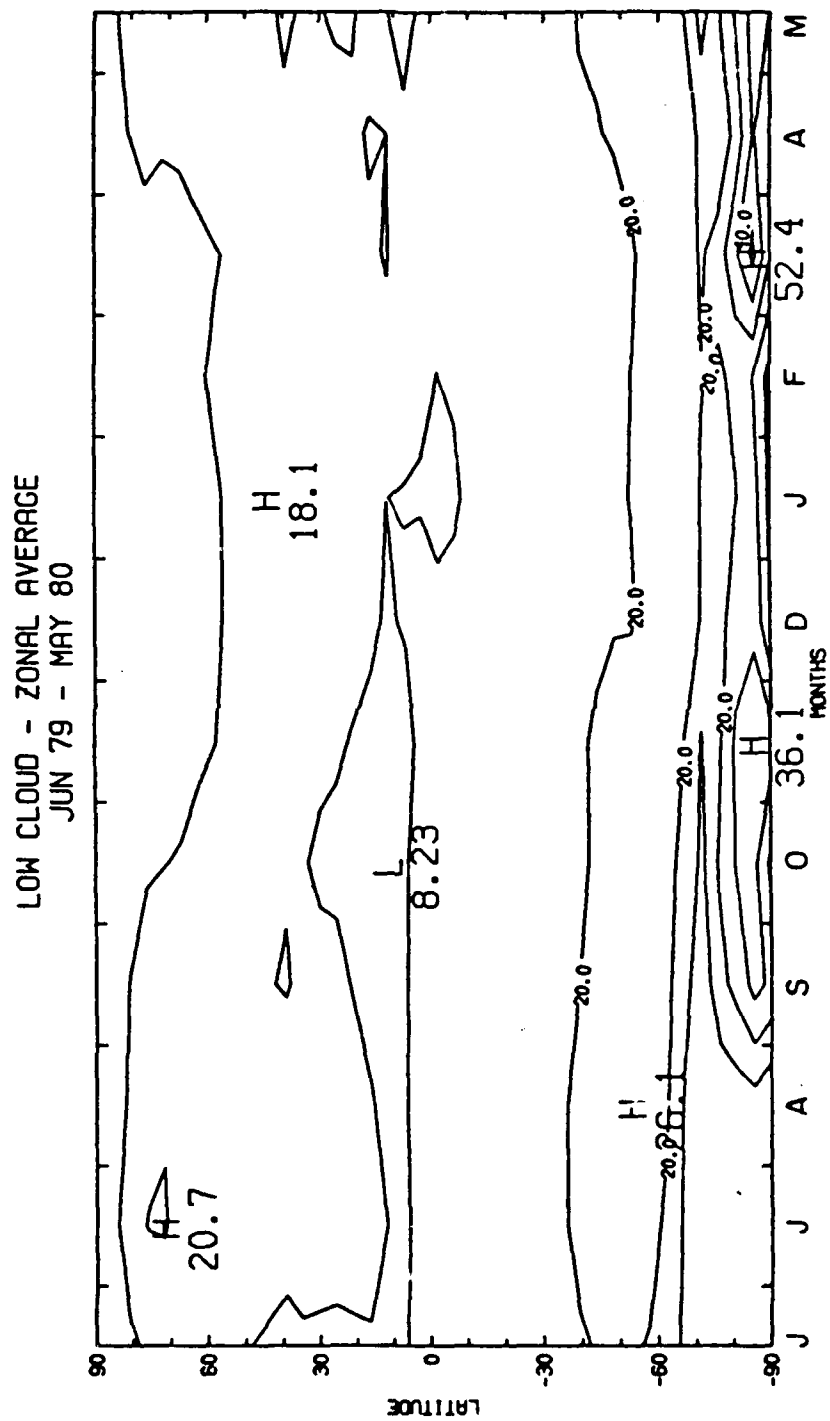

Figure C.1 Time-latitude cross section of zonally averaged total cloud amount.